Bohnhoff, M., Martinez Garzon, P., Bulut, F., Stierle, E., Ben-Zion, Y. (2016): Maximum earthquake magnitudes along different sections of the North Anatolian fault zone. - *Tectonophysics*, *674*, pp. 147—165.

DOI: http://doi.org/10.1016/j.tecto.2016.02.028

Tectonophysics 674 (2016) 147–165

Contents lists available at ScienceDirect

Tectonophysics

journal homepage: www.elsevier.com/locate/tecto

Review Article

Maximum earthquake magnitudes along different sections of the North Anatolian fault zone

Marco Bohnhoff [a,b,*], Patricia Martínez-Garzón [a], Fatih Bulut [a], Eva Stierle [a], Yehuda Ben-Zion [c]

[a] Helmholtz-Centre Potsdam GFZ German Centre for Geosciences, Telegrafenberg, 14473 Potsdam, Germany
[b] Department of Earth Sciences, Free University Berlin, Malteser Strasse 74-100, 12249 Berlin, Germany
[c] Department of Earth Sciences, University of Southern California, Los Angeles, CA 90089-0740, USA

ARTICLE INFO

Article history:
Received 30 September 2015
Received in revised form 14 February 2016
Accepted 15 February 2016
Available online 3 March 2016

Keywords:
Seismology
Historical seismicity
Continental transform faults
Fault-zone characteristics
North Anatolian fault zone
Maximum earthquake magnitude

ABSTRACT

Constraining the maximum likely magnitude of future earthquakes on continental transform faults has fundamental consequences for the expected seismic hazard. Since the recurrence time for those earthquakes is typically longer than a century, such estimates rely primarily on well-documented historical earthquake catalogs, when available. Here we discuss the maximum observed earthquake magnitudes along different sections of the North Anatolian Fault Zone (NAFZ) in relation to the age of the fault activity, cumulative offset, slip rate and maximum length of coherent fault segments. The findings are based on a newly compiled catalog of historical earthquakes in the region, using the extensive literary sources that exist owing to the long civilization record. We find that the largest M7.8–8.0 earthquakes are exclusively observed along the older eastern part of the NAFZ that also has longer coherent fault segments. In contrast, the maximum observed events on the younger western part where the fault branches into two or more strands are smaller. No first-order relations between maximum magnitudes and fault offset or slip rates are found. The results suggest that the maximum expected earthquake magnitude in the densely populated Marmara–Istanbul region would probably not exceed M7.5. The findings are consistent with available knowledge for the San Andreas Fault and Dead Sea Transform, and can help in estimating hazard potential associated with different sections of large transform faults.

Contents

* Corresponding author at: Helmholtz-Centre Potsdam GFZ German Centre for Geosciences, Telegrafenberg, 14473 Potsdam, Germany.
E-mail address: bohnhoff@gfz-potsdam.de (M. Bohnhoff).

http://dx.doi.org/10.1016/j.tecto.2016.02.028

1. Introduction

Estimates of seismic hazard depend on the maximum expected (and/or maximum possible) earthquake size in the region of interest (e.g., Field et al., 2009). However, instrumental earthquake catalogs cover only approximately 100 years, substantially less than typical recurrence times of major earthquakes (e.g., Parsons, 2004; Ben-Zion, 2008). Consequently, there is currently no reliable method for determining the hazard potential of large earthquakes along major fault systems.

Subduction zones host the largest earthquakes on Earth due to the large overall available brittle rupture surfaces (e.g., Ruff, 1996). Continental transform faults such as the San Andreas Fault in California, the Dead Sea Transform fault in the Middle East, or the North Anatolian Fault Zone in Turkey (referred to as NAFZ hereafter) tend to produce earthquakes with magnitudes M typically not exceeding ~8, releasing ~30 times less seismic energy compared to the recent mega-thrust events in Indonesia (2004 Sumatra), Chile (2010 Maule), and Japan (2011 Tohoku-Oki). Despite this fact, M8 type earthquakes along continental strike-slip faults pose a substantial seismic hazard since they can occur nearby or directly through densely populated regions such as the Los Angeles Basin, the San Francisco Bay area, or the Istanbul metropolitan region. Constraining the expected maximum earthquake size in such regions can have significant societal benefits and improve the understanding of long-term physical processes acting along major faults.

The size of large earthquakes is commonly quantified by the scalar seismic moment (Aki, 1966) $M_0 = \mu \cdot \Delta\mu \cdot A$, where $\Delta\mu$ is slip, A is the rupture area and μ is effective rigidity (typically assumed $\sim 3 \cdot 10^{10}$ Pa for crustal earthquakes). For strike-slip faults, the rupture area can be simplified as the product of rupture length and vertical depth extension. While a fraction of fault slip in the seismogenic depth range can be aseismic (e.g., Ben-Zion and Lyakhovsky, 2006; Avouac, 2015), we assume for simplicity (given the available information) that the entire 15–20 km thick seismogenic part of the crust is activated during $M > 6.5$ earthquakes. Consequently, the seismic moment and therefore the magnitude are directly related to the rupture length and the average slip. Observations indicate that plate-bounding transform faults are typically segmented, and that earthquake slip can be limited to a single fault segment, or may activate several fault segments in multi-segment failures (Sieh et al., 1993; Barka et al., 2002; Eberhart-Philips et al., 2003; Kondo et al., 2010). The rupture patterns at given locations may change and evolve on long term when individual segments combine to form a larger, more uniform, and simplified potential slip zone (Wesnousky, 1988; Ben-Zion and Sammis, 2003; Papageorgiou, 2003). In consequence, this can lead to increasing maximum magnitudes with fault-zone development.

The geometrical and structural parameters of fault zones may change with time reflecting the fault evolution from a young, short, and segmented state toward a more continuous and larger fault zone (e.g. Tchalenko, 1970; Sengör et al., 2005; Wechsler et al., 2010). The development of a strike-slip fault is reflected in several parameters such as the geological age, cumulative offset across the fault, slip rates, and length of the individual coherent segments. As a consequence of the structural development, the resulting maximum likely magnitude may also increase. The cumulative offset across the fault combines information on the fault age and the average deformation rate. The length of individual fault segments tends to increase with total offset, and hence with age, as initially small and separated segments coalesce to form larger joint segments (e.g. Wesnousky, 1988; Stirling et al., 1996).

In this study, we present and analyze a catalog of historical seismicity for the entire NAFZ in Turkey based on numerous historical and paleoseismic records. The results are discussed in relation to available information on fault age, cumulative offset, slip rates, and geometrical parameters associated with different parts of the NAFZ. The presented earthquake catalog covers the last 2300 years and appears to be complete down to M_s7.3, i.e. it is unlikely that earthquakes larger than 7.3 for the time period considered are missing in the catalog. The data compilation provides field evidence that the maximum observed earthquake magnitude along the fault increases with fault age along the eastern and central part of the fault. The cumulative offset along the fault is approximately constant, which may be partially related to slip rate changes along the fault. The larger maximum observed earthquake magnitude (M up to ~8) along the eastern NAFZ compared to the western part (M up to ~7.4) may be related to different levels of structural development. These results are in agreement with available historical and instrumental seismicity data for two other major strike-slip faults, the San Andreas Fault and the Dead Sea Transform.

2. The North Anatolian Fault Zone

The NAFZ is one of the largest currently active continental strike-slip faults in the world extending along more than 1200 km from the Karliova triple junction in the east to the northern Aegean in the west (Fig 1A). The NAFZ was described in the late 1940s (Ketin, 1948) and it is now one of the best-studied strike-slip fault zones on Earth. The fault developed in relation to the northward migrating Arabian Plate in the east and the southward rollback of the Hellenic subduction zone in the west (Armijo et al., 1999; Flerit et al., 2004; LePichon et al., 2015). The NAFZ marks a narrow fault zone along its eastern and central parts, while branching into two or three sub-parallel strands is evident west of 31°E (Fig. 1B). The current slip rates are about 20 mm/yr in the east and 25 mm/yr in the west (Barka, 1992; McClusky et al., 2000; Reilinger et al., 2006). The NAFZ sustains predominantly right-lateral strike-slip faulting mechanisms, but in the western part, normal faulting earthquakes are also observed due to the transtensional setting produced by the slab pull of the Hellenic subduction zone (Flerit et al., 2004; Bohnhoff et al., 2005). Earthquake source mechanisms indicating transpression are not observed along the entire fault zone (Fig. 1C) (Sengör et al., 2005; Ekström et al., 2012). The NAFZ provides an important natural laboratory for understanding earthquake mechanics and fault behavior over multiple earthquake cycles due to its long and extensive historical record of large earthquakes (Ambraseys and Finkel, 1987, 1991, 1995; Ambraseys, 2002). Despite the long historical record of the region, a catalog of historical earthquakes for the entire North Anatolian Fault Zone is not yet available.

Over the past centuries, the NAFZ sustained several cycle-like sequences of large-magnitude ($M > 7$) earthquakes (Stein et al., 1997). Of these, the most prominent and best studied is the sequence of the 20th century that ruptured all but the Sea of Marmara segments in a series of westward propagating events, with the most recent being the Izmit (M_w 7.4) and Düzce (M_w 7.1) earthquakes of 1999 (e.g. Parsons et al., 2000; Reilinger et al., 2000; Barka et al., 2002) (Fig. 2). In the following, we summarize information on large seismic events and on fault segments for the western, central, and eastern portion of the NAFZ. Throughout the text, we consistently refer to surface wave earthquake magnitudes (M_s) converting moment magnitudes for instrumental earthquakes to M_s following the relation proposed by Scordilis (2006) as discussed later in the text. Individual NAFZ fault sections described in the text are indicated in Fig. 1A and shown in more detail in Figs. 2–4.

2.1. Western NAFZ (26°–32°E)

The northern NAFZ branch in the west hosts most of the current deformation as determined from GPS measurements (Straub et al., 1997; Ergintav et al., 2014). Its trace is narrow and well-defined along the Marmara segment and the Ganos Fault, while the branching most likely further increases beyond the northern Aegean to the west (Fig. 2). There, no $M > 7$ earthquakes are reported in historical records. The most recent 2014 M6.9 Aegean earthquake (Bulut, 2015) fits well

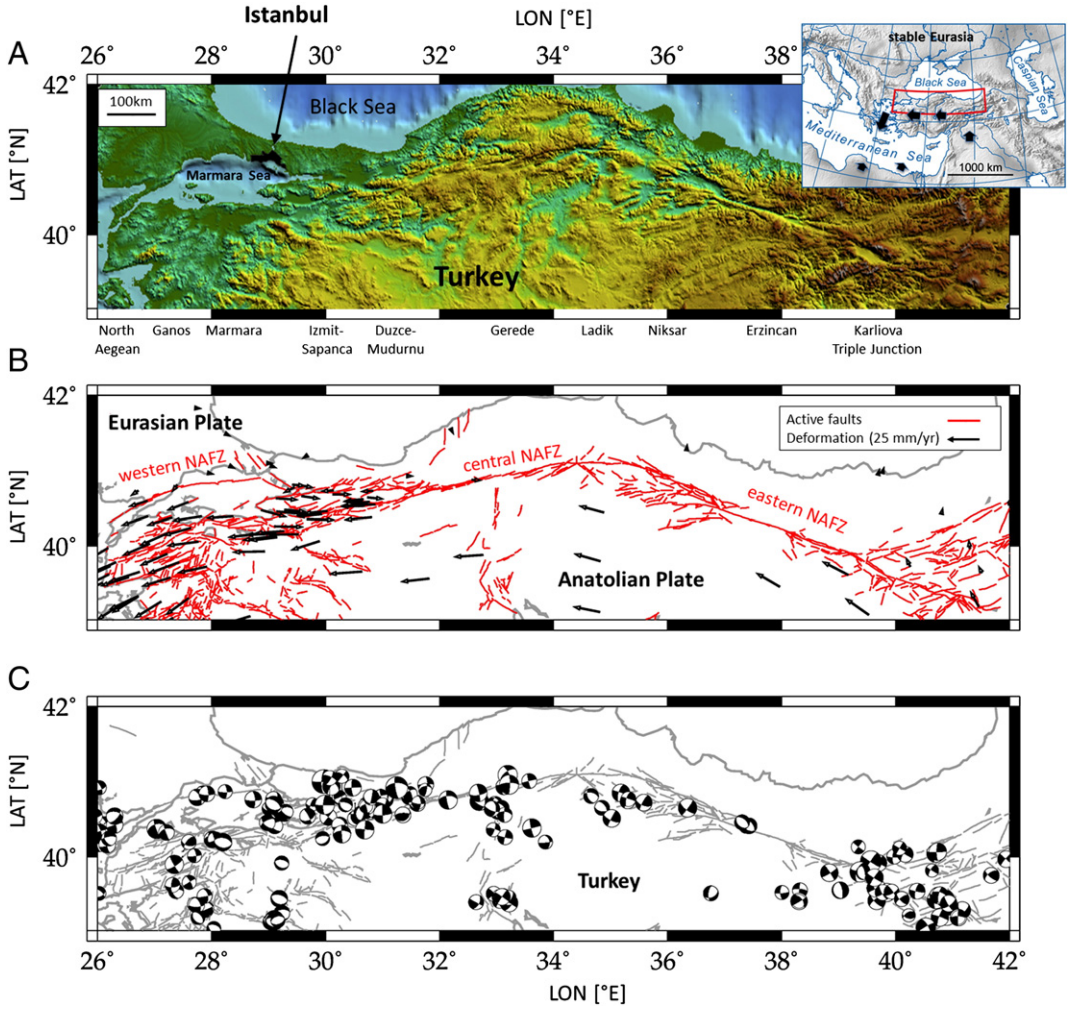

Fig. 1. Tectonic setting of the NAFZ in Turkey. The NAFZ extends from the Karliova triple junction in eastern Anatolia throughout northern Turkey toward the Istanbul–Marmara region and further into the North Aegean where it spreads into several branches. A) Topography of northern Turkey along the NAFZ reflecting a narrow fault along its eastern half between 34° and 40°E. B) Mapped fault segments of the NAFZ (red lines) (Turkey General Directorate of Mineral Research and Exploration, pers. comm.) and GPS-derived horizontal velocity field of the Anatolian plate with respect to stable Eurasia (black arrows) (after McClusky et al., 2000). C) Earthquake focal mechanisms compiled from the CMT catalog (Ekström et al., 2012) and Sengör et al. (2005) for the years 1939–2012. The inset in the upper right shows a location map of the greater eastern Mediterranean region with the bold black arrows indicating the simplified relative plate motion with respect to stable Eurasia and the red polygon indicating the study region.

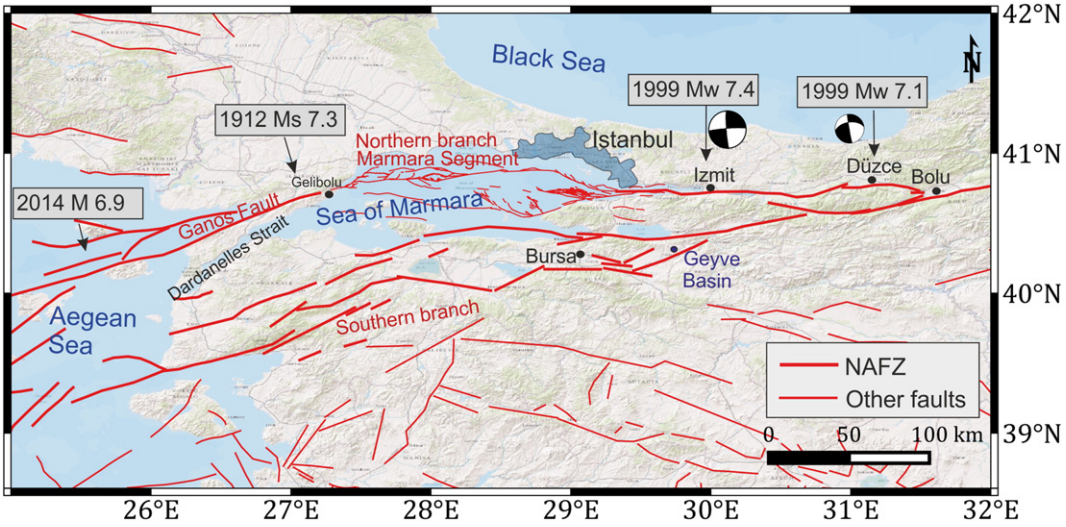

Fig. 2. Western NAFZ. Map of the western part of the NAFZ. Faults are as in Fig. 1. Major recent earthquakes are indicated by year and magnitude pointing to the epicenter. For the 1999 Izmit and Düzce events also the focal mechanisms are shown. Geographical features are explained in the text. Map created using the GIS mapping tool.

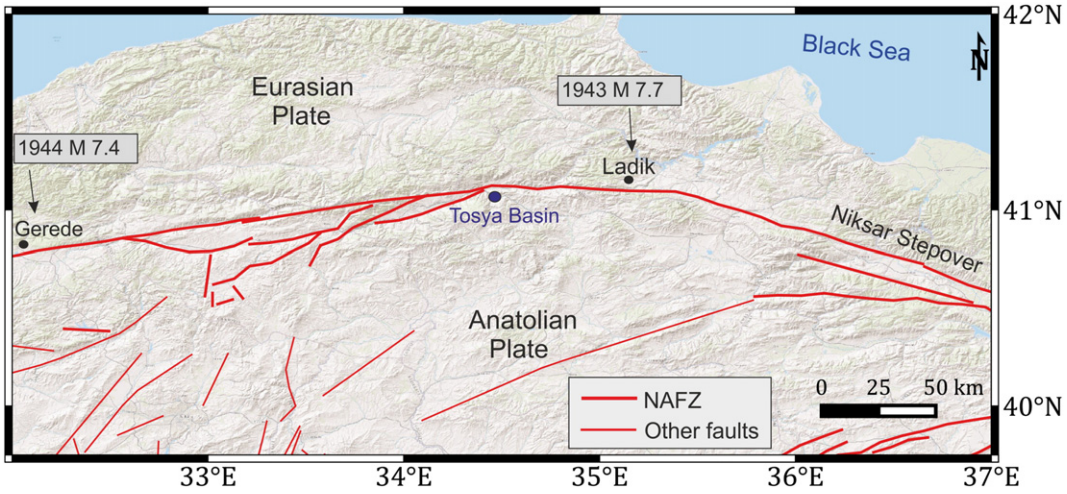

Fig. 3. Central NAFZ. Map of the central part of the NAFZ. Faults are as in Fig. 1. Major earthquakes of the 20th century are indicated by year and magnitude pointing to the epicenter. Geographical features are explained in the text. Map created using the GIS mapping tool.

in this picture. The fault-zone age is on the order of 5–7 Ma (Armijo et al., 1999; Sengör et al., 2005, see discussion below). LePichon et al. (2015) recently proposed a model for the transition of the NAFZ into the broader Aegean region and potential links to the main tectonic features, namely the Corinth rift and the Hellenic subduction zone. In this model, the Marmara region has been initially formed as part of an NS-extensional regime extending throughout western Anatolia driven by the accelerated rollback of the Hellenic subduction zone. At about 2 Ma, this regime was transferred into a strike-slip fault cross-cutting the Sea of Marmara (LePichon et al., 2015).

The onshore Ganos fault as part of the northern NAFZ branch is a 45-km-long linear fault connecting the westernmost portion of the NAFZ in the northern Aegean to the main NAFZ branch below the Sea of Marmara (e.g Janssen et al., 2009). It consists of several sub-parallel branches which are separated by less than 1 km (Okay et al., 2004; Janssen et al., 2009). The total accumulated right-lateral slip displacement since the latest Miocene is reported to be 70 km (Armijo et al., 1999). The most recent major earthquake in this region (the 1912 Ganos/Mürefte event) had a magnitude of M7.3. It ruptured the entire Ganos Fault and may have extended into the westernmost Sea of Marmara (Armijo et al., 2005). Previous major events of the region occurred in 1659, 1354, (1081), and 824 (Altinok et al., 2003). Based on GPS measurements, the current deformation rate across the main northern NAFZ strand at the Ganos fault is 20 mm/yr (Ergintav et al., 2014). Assuming the maximum displacement during the 1912 event to be typical, this would result in a recurrence period of 280 ± 20 yrs. Paleoseismic investigations along the Ganos and Izmit segments identified several seismic events. No indications have been found from trenching studies that an earthquake larger than M7.4 occurred along this part of the NAFZ during the past millennium (Rockwell et al., 2009).

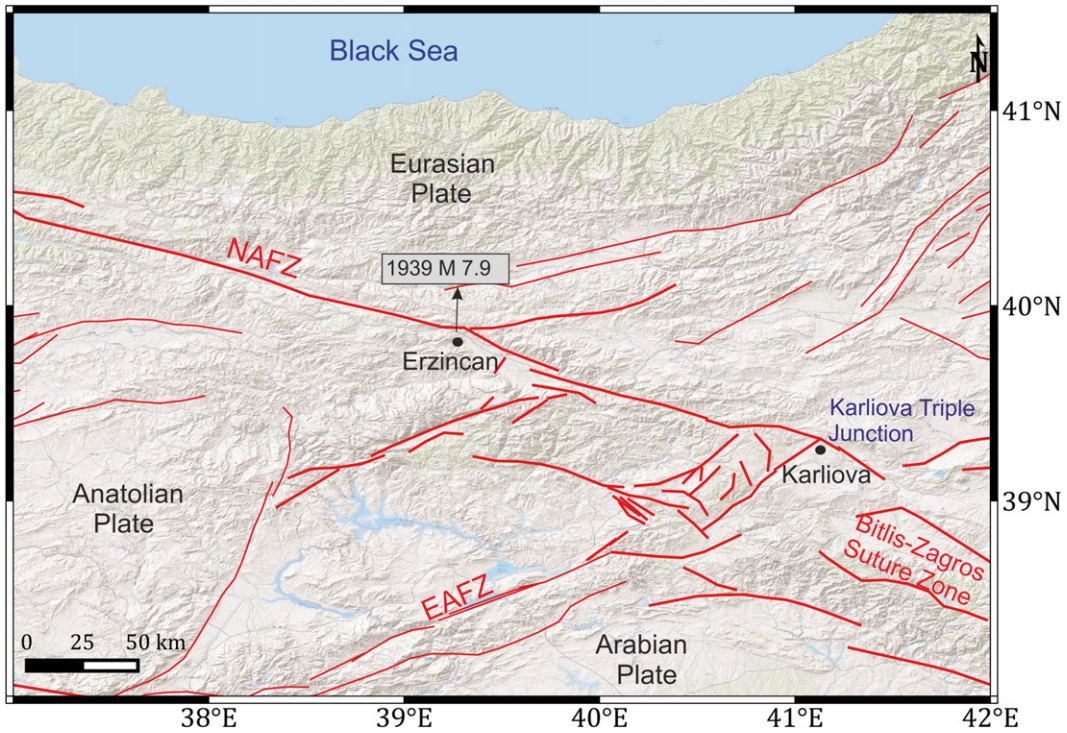

Fig. 4. Eastern NAFZ. Map of the eastern part of the NAFZ. Faults are as in Fig. 1. The 1939 Erzincan earthquake is indicated by year and magnitude pointing to the epicenter. Geographical features are explained in the text. Map created using the GIS mapping tool.

In the western Marmara region, more than 300 destructive earthquakes have occurred during the last 41 centuries, the largest eight of which were about M 7.4 and occurred at intervals of 150–420 years (Ambraseys, 2002). These upper bounds for magnitudes are indicated by the projected maximum fault rupture lengths and assuming common estimations for average coseismic slip of 2–3 m during the larger earthquakes. Since the rupture lengths could not have exceeded ~200 km based on trenching results throughout the region, we infer that an upper bound for the earthquake magnitude along the entire western portion of the fault is 7.5. The Marmara segment of the NAFZ has not been activated in a major earthquake since 1766. If fully locked, as suggested for the western portion of the Marmara seismic gap from recent microseismicity (Bohnhoff et al., 2013) and GPS data (Ergintav et al., 2014) it might have accumulated a slip deficit of 2.5–3.7 m since then.

Trenching results from the Izmit segment east of the Sea of Marmara suggest a recurrence period of ~150 years. This recurrence period is substantially shorter than along the Ganos segment (Rockwell et al., 2009) and it would be in accordance with the Izmit segment hosting most of the deformation of the fault zone, while the Ganos segment is located in one of the two or even more branches of the NAFZ in that region. Klinger et al. (2003) studied the rupture history of the NAFZ near Izmit, and they determined that the fault had ruptured only three times since the fifteenth century. They attributed the surface ruptures to the M ≤ 7.5 events of 1509, 1719, and 1999, while the coseismic slip along the segments throughout NW Turkey was found to be up to 4–5 m at the trenched sites. The history of the ruptures identified from trenching along the Izmit segment suggests similar offsets for the identified events and a nearly periodic rupture (Klinger et al., 2003).

2.2. Central NAFZ (32°–~37°E)

Trenching results along the Gerede segment that hosted the 1944 M 7.4 Bolu–Gerede earthquake indicate a repeated slip along this part of the NAFZ with five events since 643 B.C., and the fault geometry exhibits highly linear traces suggesting a well-developed and smoothed fault zone (Kondo et al., 2010) (Fig. 3). The same authors concluded that slip of all five events probably was similar and that the events were multi-segment earthquakes. Cumulative slip along the 1944 Bolu–Gerede rupture identified from trenching results is in the range of 25 m for the past 1500 years accounting for approximately 16 mm/yr and thus significantly lower than that interpreted from GPS data (Okumura et al., 2004; Rockwell et al., 2004; Kondo et al., 2010). This is different than for the Marmara region where no such deficit is observed and might indicate some extent of near-surface creep along this segment.

The Ladik section as the next fault segment to the east ruptured in the 1943 M 7.7 Ladik earthquake and activated a 280-km-long fault segment (Ambraseys, 1970; Barka, 1996) (Fig. 3). The penultimate event on this fault segment may have been the 1794 (Ambraseys and Finkel, 1995) or the 1668 mega earthquake that ruptured from Erzincan to Bolu (Sengör et al., 2005). Interestingly, the 1943 event has not been identified in the stratigraphy in contrast to the earlier and most likely even larger earthquakes along this part of the NAFZ. This correlates well with calculating the cumulative displacement for the last 2300 years based on rupture displacements similar to the 1943 event that would correspond to a slip rate of ~6 mm/yr and thus would result in a substantial slip deficit since there is no indication for creep along this segment. As a result, paleo-earthquakes here likely might have been larger than M7.4 (Fraser et al., 2009). At Lake Ladik, Fraser et al. (2009) identified a total of seven large earthquakes over the past 3000 years prior to the 1943 event (Fig. 3) with an estimated inter-event time of 385 ± 166 years.

The Niksar step-over limits the central NAFZ to the east (Figs. 3 and 4). There, trenching reveals evidence for four, possibly five, surface ruptures during the past 2300 years, as well as one much older event (Hartleb et al., 2003). The 10-km-wide Niksar step-over is of great relevance for its role as a seismic barrier to the rupture of large regional events such as the 1668 earthquake (Ambraseys and Finkel, 1988). This step-over also terminated the 1939 Erzincan (M_S 7.8–8.0) rupture to the west. The 17 August 1668 event (Ambraseys and Finkel, 1988) was defined as one of the largest earthquakes associated with the North Anatolian Fault Zone. It caused heavy damage within an about 100-km-wide and 600-km-long region, rupturing the fault zone between Bolu/Gerede in the west (Fig. 2) and Erzincan in the east (Albini et al., 2013) (Fig. 4). According to this, at least one-third of the entire known length of NAFZ broke during this event. The length of the rupture zone and the associated fault slip provides a rationale for a magnitude of 7.8–8.0 for this earthquake (Ambraseys and Finkel, 1988).

2.3. Eastern NAFZ (~37°–40°E)

Kozaci et al. (2011) identified seven events along the eastern NAFZ section for the past 2000 years concluding that their paleo-earthquake data reinforced the idea of relatively infrequent, large-magnitude events. They attributed this relatively simple behavior to the structural maturity of the NAFZ and its relative isolation from other major seismic sources within the Anatolia–Eurasia boundary. This suggests that this part of the NAFZ might represent a well-developed fault zone being capable of producing multi-segments ruptures resulting in earthquakes as large as M 8.0. We refer to this later in the text. The Erzincan section as the easternmost portion of the NAFZ represents the oldest part of the entire fault zone and formed ~12–13 Ma ago (Dewey et al., 1989; Sengör et al., 2005) (Fig. 4). Since this area is less populated than the broader Marmara region, historical data are less abundant but suggest that the eastern part of the NAFZ probably ruptured in a series of large earthquakes during the middle-to-late sixteenth century (Hartleb et al., 2003). Erzincan itself, representing the largest city in direct vicinity to the eastern NAFZ, was heavily damaged in major earthquakes in 1543, 1579, and 1590 and was completely destroyed in the 1583 earthquake (Ambraseys and Finkel, 1995). The NAFZ reaches its easternmost part in the Karliova triple junction where the fault converges with the East Anatolian Fault Zone and the Bitlis–Zagros Suture Zone (Fig. 4).

3. Parameters of different sections of the NAFZ

3.1. Fault Age

The westward extrusion of the Anatolian Plate started 12–13 Ma ago during the late phase of collision between Arabia and Eurasia (Dewey et al., 1989). This process is directly linked to the onset of motion of the NAFZ that started in the east and then propagated westward. The youngest reported fault-zone age is 0.2–2 Ma for 30–32°E (Sengör et al., 2005) (Fig. 5, Table 1). However, this value might not be representative of the main fault zone in this region but could possibly relate to secondary fault branches of age younger than the main fault zone. Further westwards in the Marmara region/Aegean extensional regime age values are reported to be 6–8 Ma (Armijo et al., 1999), while a value less than 1 Ma is also reported (Sengör et al., 2005, see above). The estimated fault-zone ages generally have large error bars along most of the fault except for its easternmost (oldest) portion (Fig. 5, Table 1). Although somewhat older basins exist along northern Turkey, only the late Miocene–Pliocene basins within the NAFZ are clearly related to deformation along the currently active fault zone (Barka, 1992). In northwestern Turkey, it is in part difficult to clearly differentiate between age markers that are related to the currently active NAFZ from earlier (pre-NAFZ) deformation phases. Furthermore, the NAFZ activity in northwestern Turkey might have formed at 6 ± 2 Ma as a dominantly NS-extensional system that later evolved into a strike-slip fault (LePichon et al., 2014, 2015). Such a view would in part explain the broad range of observed fault-zone age and also offset

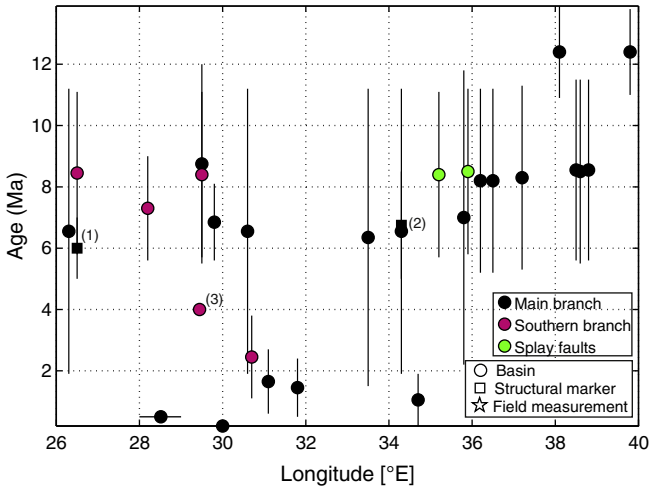

Fig. 5. NAFZ fault-zone age. Fault-zone age for major basins and fault strands along the NAFZ from west to east. Most data comes from the age of the basins described in Sengör et al. (2005) and therefore they represent a minimum estimate. Superscripts (1), (2), and (3) refer to estimates from Armijo et al. (1999); Hubert-Ferrari et al. (2002) and LePichon et al. (2014, 2015). Largest values for the age of the NAFZ are reported for the eastern part decreasing westward. Youngest sections are located between 30 and 32°E while for the westernmost part of the NAFZ non-uniform values are reported. Black symbols correspond to basins on the main NAFZ strand. Blue symbols correspond to the southern NAFZ strand. Green symbols refer to information from splay faults. The dot crossed with a horizontal bar at 28.5 refers to the overall minimum value of 0.2 Ma for the Marmara region (Sengör et al., 2005). Shaded areas mark the extensional Aegean regime and the westward decreasing average age (Armijo et al., 1999; Sengör et al., 2005), respectively.

across the fault (see next section) In contrast to a reported minimum fault-zone age of only 225 kyr (Sengör et al. (1985, 2005) in conjunction with observed small fault offsets of only 4 km at the western margin of the Central Basin of the Sea of Marmara (LePichon et al., 2001, 2003) and a similar offset in the Central High (Armijo et al., 2002; LePichon et al., 2003) (Table 2; Fig. 6), cumulative offsets of 70 km and more are reported for the same region (Armijo et al., 1999; Hubert-Ferrari et al., 2002) (see next section). The largest age might represent the overall cumulative value for the fault zone while the smaller values might represent younger secondary branches. In summary, the fault-zone age is decreasing along most of the fault (~30–40°E) from 12 to 13 Ma in the east to several (up to 6–8) Ma at 30°E, with the age of the western NAFZ being heavily disputed. The Aegean extensional system might have dominated the fault-zone development, and the overall fault-zone age might be as large as 8 Ma.

3.2. Cumulative offset

The cumulative fault displacement along the NAFZ has been a matter of debate for some years. Armijo et al. (1999) and Hubert-Ferrari et al. (2002) report values for cumulative offsets across the NAFZ obtained from structural and morphological markers between ~30 and ~80 km with no systematic variation along the NAFZ (Table 2, Fig. 6). In contrast, Sengör et al. (2005) based on different geological and geomorphological markers reported that the cumulative offset is decreasing from up to ~90 km in the east towards only 25–40 km in the west, and at its central part the offset is 30–75 km (Table 2, Fig. 6).

For example, the geometry of the Yesilirmak River suggests a total offset of ~30 km and >50 km at different locations, while a proposed stream-capture scenario for this same area indicates a total offset of as much as 75 km (Hubert-Ferrari et al., 2002). The reported average total offset in the Sea of Marmara extends from values as small as only ~30 km (Sengör et al., 2005) to 70 km at the Ganos fault (Armijo et al., 1999). As a result of these large discrepancies from the different measurements, reported smaller values for the cumulative offsets across the NAFZ might not represent the total offset but instead offsets of secondary branches or offset of features (e.g. rivers) formed after the fault formation. In summary, the largest reported values for the cumulative offset across the NAFZ do not show a systematic variation along the fault. Consistent values with up to 90 km offset are reported only for the easternmost part where the fault is 12–13 Ma old. To further elaborate on the evolution of the NAFZ, one additional source of

Table 1
NAFZ fault-zone age (table updated with respect to initial submission).

Lat	Lon	Age min (Ma)	Age max (Ma)	Age Ø (Ma)	Name	Branch	Reference
40.6	26.5	5	7	6	Dardanelles	Main	Armijo et al., 1999
40.5	26.3	1.9	11.2	6.55	Gelibolu Basin	Main	Sengör et al., 2005
40	26.5	5.8	11.1	8.45	Bayramic (Etili) Basin	Southern	Sengör et al., 2005
40.4	30	0.2	0.2	0.20	Sea of Marmara basins	Main	Sengör et al., 2005
40.4	28.2	5.6	9.0	7.30	Manyas-Ulubat Basin	Southern	Sengör et al., 2005
40.6	29.5	4.0	4.0	4.00	Southern shelf Sea of Marmara	Southern	LePichon et al., 2014, 2015
40.6	29.5	5.5	12.0	8.75	Yalova Basin	Main	Sengör et al., 2005
40.3	29.5	5.7	11.1	8.40	Yensehir Basin	Southern	Sengör et al., 2005
40.5	29.8	5.6	8.1	6.85	Gölcük-Derince Basin	Main	Sengör et al., 2005
40.7	30.6	1.9	11.2	6.55	Adapazan Basin	Main	Sengör et al., 2005
40.4	30.7	1.1	3.8	2.45	Pamukova Basin	Southern	Sengör et al., 2005
40.8	31.1	0.6	2.7	1.65	Düzce Basin	Main	Sengör et al., 2005
40.6	31.8	0.5	2.4	1.45	Bolu Basin	Main	Sengör et al., 2005
41	33.5	1.5	11.2	6.35	Cerkes-Kursunlu Basin	Main	Sengör et al., 2005
40.9	34.3	1.9	11.2	6.55	Tosya Basin	Main	Sengör et al., 2005
40.9	34.3	5.0	8.5	6.75	Pontus Formation (Tosya B.)	Main	Hubert-Ferrari et al., 2002
41	34.7	0.2	1.9	1.05	Kargi Basin	Main	Sengör et al., 2005
40.7	35.2	5.7	11.1	8.40	Merzifon Basin	Splay	Sengör et al., 2005
41.3	35.8	2.2	11.8	7.00	Vezirköprü Basin	Main	Sengör et al., 2005
40.4	35.9	5.8	11.2	8.50	Kazova Basin	Splay	Sengör et al., 2005
41.2	36.2	5.2	11.2	8.20	Havza-Ladik Basin	Main	Sengör et al., 2005
40.5	36.5	5.2	11.2	8.20	Tasova-Erbaa Basin	Main	Sengör et al., 2005
40.6	37.2	5.3	11.3	8.30	Niksar Basin	Main	Sengör et al., 2005
40.4	38.6	5.5	11.5	8.50	Susehri Basin	Main	Sengör et al., 2005
39.8	38.1	10.9	13.9	12.40	Karnos Basin	Main	Sengör et al., 2005
39.8	38.8	5.6	11.5	8.55	Bicer Basin	Main	Sengör et al., 2005
39.7	38.5	5.6	11.5	8.55	Refahiye Basin	Main	Sengör et al., 2005
39.8	39.8	11.0	13.8	12.40	Erzincan Basin	Main	Sengör et al., 2005

Fault-zone age for major basins and fault strands along the NAFZ from west to east after Armijo et al. (1999); Hubert-Ferrari et al. (2002); Sengör et al. (2005) and references therein. Given are the minimum and maximum reported values for the age as well as an average value that is referred to later in the text. See also Fig. 5.

Table 2
NAFZ cumulative fault-zone offset (table updated with respect to initial submission).

Northern—main branch								
Lon min	Lon max	Lon avg	Cum offset	Cum min	Cum max	Reference	Marker type	Comments
26	26.5	26.25	70	70	70	Armijo et al., 1999	Structural	Dardanelles folds
27	27.5	27.25	40	35	45	Okay et al., 1999	Geological	Ganos fault (minimum estimation)
27.6	27.8	27.7	4	3	5	LePichon et al., 2001	Morphological	
28	28.5	28.25	58	58	59	Yaltırak, 2002	Structural	East Marmara
30	31	30.5	85	85	85	Armijo et al., 1999	Structural	Eastern Marmara Sea, Sakarya River
31	31	31	59.5	52	67	Akbayram et al., 2016	Geological	Cretaceous Faults subperpendicular to NAF-N
33	33.5	33.25	80	65	95	Hubert-Ferrari et al., 2002	Morphological	River Gerede + Capture scenario
34	34	34	80	70	90	Hubert-Ferrari et al., 2002	Structural	Tosya Basin
34.5	35	35	80	80	80	Hubert-Ferrari et al., 2002	Morphological	Kizilirmak River + Capture scenario
34.5	35	35	30	30	30	Barka, 1992	Morphological	Kizilirmak River
34.5	35	35	40	35	45	Sengör et al., 2005	Morphological	Kizilirmak River
35.6	36.2	35.9	30	25	35	Sengör et al., 2005	Morphological	Turhal–Amasya Plain
36	36.5	36	75	10	75	Hubert-Ferrari et al., 2002	Morphological	River Yesilirmak + Capture scenario
36	36.5	36	50	50	75	Sengör et al., 2005	Morphological	Amasya Plain–Lâdik deflection
36	36.5	36.25	80	75	85	Barka et al., 2000	Geological	Offsets from Niksar + Tasova–Erbaa Basin
38.5	39	38.75	85	80	90	Seymen's, 1975	Morphological	Suture Zone Refahiye
38	40	39	85	65	110	Hubert-Ferrari et al., 2002	Structural	Pontide Suture
39.5	40	39.75	70	65	75	Sengör et al., 2005	Morphological	Karasu
39.9167	40.3167	40	65	65	65	Hubert-Ferrari et al., 2002	Morphological	Euphrates River
Southern branch								
Lon min	Lon max	Lon avg	Cum offset	Cum min	Cum max	Reference	Marker type	Comments
26	26.5	26.25	20	15	25	Armijo et al., 1999	Structural	Dardanelles folds
28	28.5	28.25	18	17	19	Yaltırak, 2002	Structural	Gemlik + Bursa
30	30.5	30.25	30	30	80	Westaway, 1994	Morphological	Sakarya River
30	30.5	30.25	24	22	26	Koçyiğit, 1988	Geological	Geyve Basin
33.25	33.75	33.5	50	45	50	Herece and Akay, 2003	Geological	Eocene-aged volcanics Gerede-Ilgaz

Cumulative fault offset across the NAFZ from west to east. Given are the minimum and maximum reported values for the offset as well as an average value that is referred to later in the text. See also Fig. 6.

information can be deduced from reconstructing slip rates along the fault. While a constant slip rate would suggest a decreasing offset in the west (given the older age in the east), slip rates being smaller in the east might result in a semi-uniform cumulative offset across the fault along strike.

3.3. Slip rates

Several studies have estimated the slip rates of the NAFZ using different approaches and focusing on different spatial and temporal scales (Fig. 7). GPS-based estimates for slip rates along the entire NAFZ covering the last few decades indicate an increase from 20 mm/yr in the east to as much as 25 mm/yr in the west (McClusky et al., 2000; Reilinger et al., 2006) with lower values for the northern and southern fault strands in the Marmara region (Straub et al., 1997; Ergintav et al., 2014), which is well-explained by fault-zone branching. Results from geomechanical modeling indicate slightly lower values around 15 mm/yr (Hergert and Heidbach, 2010).

Armijo et al. (1999) estimated the 5 Ma average slip rate necessary to accumulate the observed 70 km cumulative displacement at Gelibolu to be 17 mm/yr. This suggests that the average slip rate for the entire NAFZ in northwestern Turkey may have accelerated over time toward the current average slip rate of close to 30 mm/yr in the northern Aegean (McClusky et al., 2000; Reilinger et al., 2006).

Average long-term values of the slip rate for 5 and 13 Ma using geological structures give 17–19 and 6.5 mm/yr across the NAFZ in the west and east, respectively (Armijo et al., 1999; Hubert-Ferrari et al., 2002). Although there is some variability between these studies, most of them lay within the corresponding confidence intervals and they show the same trend as for the entire fault: current slip rates of 20–25 mm/yr are significantly larger than those estimated for the long term (~6.5–17 mm/yr). The same feature is observed for the central NAFZ where slip rates for >1 ky are estimated to be 17–18.5 mm/yr (Hubert-Ferrari et al., 2002) while GPS measurements indicate ~25 mm/yr (Yavaşoğlu et al., 2011; Tatar et al., 2012). For the eastern section of the NAFZ, long-term average slip rate estimates obtained from the offset of geological structures give 6.5 mm/yr over the last 13 Ma (Hubert-Ferrari et al., 2002). Recent estimation from GPS and INSAR vary between 16 and 20 mm/yr (Özener et al., 2010; Tatar et al., 2012; Walters et al., 2014).

Interestingly, the different reported average slip rates along different sections of the NAFZ are consistent with comparable cumulative offsets of ~85 km in the western and eastern fault portions (see discussion below). In summary, there is an increase of slip rate in time along the entire NAFZ in combination with a currently higher slip rate in the west (25 mm/yr) compared to the east (20 mm/yr).

3.4. Individual fault segments

In this study, individual mapped fault segments are defined to represent quasi-linear portions of the main fault zone with minimum step-over distance of 5 km to the most adjacent fault segment. This step-over distance was chosen since earthquake ruptures are seen to terminate if the step-over distance is larger than 5 km (e.g. Harris et al., 2002; Lettis et al., 2002). In the Marmara and North Aegean region, the NAFZ segments are generally much shorter relative to the main central and eastern part of the fault zone (Barka, 1992). The fault is mainly a single trace between Karliova and the Mudurnu valley while the NAFZ branches into at least two strands toward the Marmara region. Coherent segments reach up to 90 km length in the eastern part along the Erzincan area (Barka, 1992) (Table 4). The maximum individual fault segment length generally decreases from Eastern Anatolia towards the west, where the major NAFZ branches typically display 20–40-km-long segments while also individual segments reach lengths on the order of 40–60 km (Fig. 8) (Barka, 1992; Barka et al., 2002). This is supported by co- and post-seismic observations in the Izmit–Düzce region and probably also below the Sea of Marmara (Bohnhoff et al., 2006, 2013).

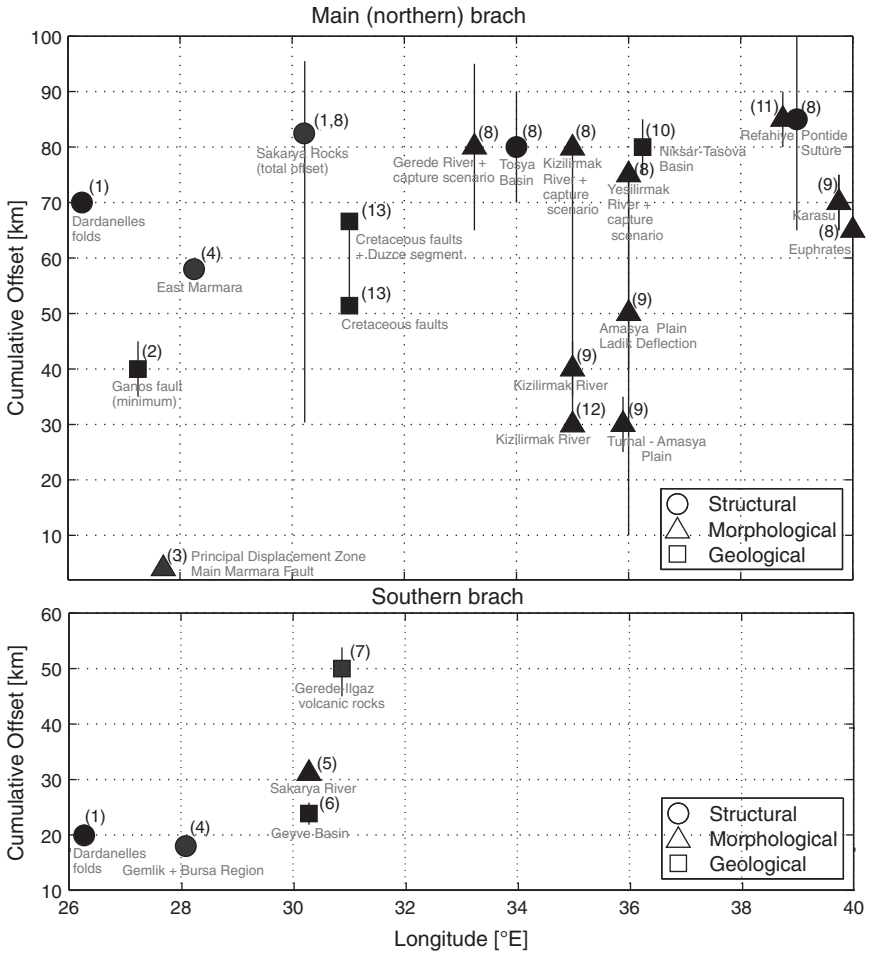

Fig. 6. Cumulative fault-zone offset across the NAFZ Cumulative offset across the NAFZ from west to east for a) the northern and main branch and b) the southern branch in the west. Superscripts represent the reference for the corresponding offset estimation: (1) Armijo et al. (1999), (2) Okay et al. (1999), (3) LePichon et al. (2001), (4) Yaltırak (2002), (5) Westaway (1994), (6) Koçyiğit (1988), (7) Herece and Akay (2003), (8) Hubert-Ferrari et al. (2002), (9) Sengör et al. (2005), (10) Barka et al. (2000), (11) Seymen's (1975), (12) Barka (1992), (13) Akbayram et al. (2016) after Armijo et al. (1999); Hubert-Ferrari et al. (2002); Sengör et al. (2005) and references therein. Offset values generally show a non-uniform trend along the trend where values at all except the easternmost part of the NAFZ show a large variation between a few tens (or even less) and 80–90 km. Black symbols correspond to values across the entire fault zone. Blue symbols correspond to an individual major (i.e. northern or southern) NAFZ branch. Circles, triangles, and squares mark structural, morphological, and geological markers, respectively. Note that some of them are minimum estimations (see Table 2 for details). Vertical bars mark estimated range of offset values at the given locations.

4. Historical seismicity catalog and geometrical fault parameters

Turkey has one of the longest and best documented historical earthquake records in the world due to several thousand years of civilization and remarkably full and continuous literary sources (Ambraseys, 1970; Ambraseys and Finkel, 1995; Ambraseys and Jackson, 1998; Grünthal and Wahlström, 2012). In particular, this refers to the western part of Turkey with the cultural hub Istanbul, formerly Constantinople and Byzantium, with a settlement history dating back to ~685 B.C. The historical earthquake record of the Marmara Sea region is rivaled only by that of a few, well-documented districts in China (Ambraseys and Finkel, 1991). Here, we compile a refined seismicity catalog of historical earthquakes along the entire NAFZ from many available literature sources (Arinci, 1945; Öcal, 1968; Allen, 1969; Kárník, 1971; Ambraseys and Finkel, 1987, 1988, 1991, 1995; Ambraseys, 1970, 2002; Barka, 1992, 1996; Ambraseys and Jackson, 1998; Grosser et al., 1998; Parsons et al., 2000; Hartleb et al., 2003; Tan et al., 2008; Rockwell et al., 2009; Kondo et al., 2010; Kozaci et al., 2011; Grünthal and Wahlström, 2012). We used earthquakes occurring as early as the year 342 B.C. for which location and magnitude were provided. Connecting the historical records of ancient earthquakes in Turkey collected in various literature sources with paleoseismic results from trenching provides refined and better constrained location and magnitude for several key-events.

When different magnitudes were reported for the same event, we select the one calculated with the most advanced technique but we considered all available data to estimate the magnitude uncertainty. We consistently use the surface wave magnitude M_S determined from surface wave amplitudes since this is the most common one in the historical earthquake catalogs for the NAFZ. Estimated moment magnitudes M_W (for earthquakes that have occurred within instrumental period) were transformed to M_S using the relation of Scordilis (2006) for $6.2 \le M_s \le 8.2$:

$$M_W = 0.99(\pm 0.02) \cdot M_S + 0.08(\pm 0.13), \quad (1)$$

which is simplified to

$$M_S \approx M_W - 0.1. \quad (2)$$

Given the strict documentation of the best-reported historical events, the uncertainties of these earthquakes were assigned according to their magnitude as well as the date of the event. If the event occurred after the year 1600 A.D., we estimate that the precision is as good as 0.4/

Table 3
Slip rates along the NAFZ (table updated with respect to initial submission).

Lon min	Lon max	Slip rates (mm/yr)	Slip min	slip max	Time span	Procedure	Place	Reference
26	26.2	10.4	7.9	12.9	10–15 ky	Reliable piercing points	Gulf of Saros	Gasperini et al., 2011
26.7	27	17	12	22	1ky	Radiocarbon dating	Ganos Fault	Meghraoui et al., 2012
27	30	22	19	25	1995–2005	GPS observations	Marmara Sea region	Straub et al., 1997
27.5	27.5	14	14	14	5 My	Cumulative offset Gelibolu	Northern branch North Anatolia	Armijo et al., 1999
27.5	27.5	17	17	17	5 My	Cumulative offset Gelibolu	Anatolia—Eurasia	Armijo et al., 1999
30.2	32	15	11.8	18.3	20–60 ky	Offset geomorphic markers	Duzce Fault Segment	Pucci et al., 2008
26	40	24.1	23.1	25.1	1988–1997	GPS observations	Anatolia–Eurasia	McClusky et al., 2000
28.5	29.5	18.5	18.5	18.5	500 ky	Seismic reflection data	Cinarcik Basin	Kurt et al., 2013
28.5	29.5	17.4	15.1	19.7	405–490 ky	Mass transport deposits	Western High Marmara fault	Grall et al., 2013
29.5	30	18.6	15.3	22.1	3 ky	Cosmogenic dating 10Be	Tahtaköprü	Kozacı et al., 2009
36	40	6.5	6.5	6.5	13 Myr	Offset of river valleys / structural markers	Eastern NAFZ	Hubert-Ferrari et al., 2002
26	30	17	17	17	13 Myr	Offset of river valleys / structural markers	Western NAFZ	Hubert-Ferrari et al., 2002
29.2	29.7	9.3	7.4	11.2	10–15 ky	Reliable Piercing Points	Gulf of Izmit	Gasperini et al., 2011
32	36	20.5	15	31	2–2.5 ky	Central NAFZ	Cl36 Geochronology	Kozaci et al., 2007
33.5	33.5	18.5	15	22	10–12 ky	Morphological offset Eksik / Bercin	Eksik, Bercin	Hubert-Ferrari et al., 2002
33.5	33.5	17.75	12.5	23	~1–5 ky	C14 dating / Stream channel offset Ücoluk creek	Bercin	Hubert-Ferrari et al., 2002
36	40	20	17	23	Current	InSAR data	Easter Turkey	Walters et al., 2014
28.5	29.5	12.5	10	15	1995–2005	GPS observations	Princess Islands	Ergintav et al., 2014
29.5	30.5	25	23	27	1995–2005	GPS observations	Izmit segment	Ergintav et al., 2014
26	27.5	20	19	21	1995–2005	GPS observations	Ganos segment	Ergintav et al., 2014
27	29.5	15.3	12.8	17.8	2005–2015	3D Geomechanical modeling	Main Marmara Fault	Hergert and Heidbach, 2010
26	40	25.5	24.5	26.5	1988-2005	GPS observations	Whole fault	Reilinger et al., 2006
36	37	24	21.9	26.9	2006–2008	GPS observations	Central–Eastern Turkey	Tatar et al., 2012
39	40	16.3	14	18.6	2006–2008	GPS observations	Eastern Turkey	Tatar et al., 2012
32	36	20.1	18.7	21.5	2001–2005	GPS observations	Central Turkey	Yavaşoğlu et al., 2011
38	42	20	16	24	2003	GPS observations	Eastern Turkey	Özener et al., 2010

Slip rates along the NAFZ from west to east. Given are the minimum and maximum reported values for the offset as well as an average value that is referred to later in the text. See also Fig. 7.

0.3/0.2/0.15 and 0.1 for magnitudes up to M_S 6.0/7.0/7.5/7.8 and above 7.8, respectively. For the earthquakes that occurred previously to this date, uncertainties are higher.

Our compiled historical catalog for the NAFZ includes a total of 217 events with M > 6 covering a period of ~2300 years and therefore, multiple earthquake cycles (Table 5). The longest recurrence interval identified along the entire NAFZ based on trenching studies is 685 years (Kozaci et al., 2011), suggesting that no major (M > 7.3) earthquake is missing in the ~2300 years historical earthquake catalog. Several trenching studies report on segments from the NAFZ that sustained large earthquakes during the last 2300 years. These events are similar in size to those documented in the catalog, but since they have no verified magnitude, they are not considered here. A recurrence period >2300 years along a fault zone with an average deformation rate as large as 22 ± 3 mm/yr can probably be ruled out.

The magnitude-frequency distribution of the catalog of historical events shows a change in the slope between M_S 7.1 and 7.3 (Fig. 9a). Since there are only a few tens of events with M > 7.1, it is difficult to calculate a statistically reliable magnitude of completeness (Mc) for this catalog reflecting the entire length of the NAFZ. To better estimate Mc, we increase the number of earthquakes by adding artificial events with half and full standard deviation above and below than the respective magnitude. This results in a synthetic set of 1085 events for which the magnitude frequency is plotted in Fig 9b. The assumed conservative estimate of Mc~7.3 is confirmed and becomes clearer in the change of slope around that value. We thus use in the following M 7.3 as the magnitude of completeness of the historical earthquake catalog for the NAFZ. Several smaller events are included mainly from the western part of the fault zone due to the extended settlement history in the greater Istanbul region. Therefore, the regional magnitude of completeness for the NAFZ section west of 32°E is lower than for the NAFZ section east of 32°E (Fig. 9c + d). It is reasonable to conclude that the catalog of historical earthquakes compiled in this study is representative for the entire length of the NAFZ from the Karliova triple junction in the east to the North Aegean Sea in the west and that no M > 7.3 earthquake is missing (especially along the western section, although several such events might not be included for the eastern section).

One important parameter which may influence the earthquake magnitude for M > 6.5 events along strike-slip faults is the thickness of the seismogenic crust, which is directly related to the area ruptured in an earthquake. To determine the seismogenic depth along the NAFZ, we used local microseismicity studies (Grosser et al., 1998; Bulut et al., 2007; Yolsal-Çevikbilen et al., 2012) and calculated the thickness of the seismogenic layer as the depth down to which 90% of all local earthquakes occur. With values between 14 and 16 km (±2 km) only minor and insignificant variations were identified along the NAFZ. We also compiled information on the surface rupture length (R_l) of the historical earthquakes from the literature if it was reasonably well constrained. We then calculated a regression line between M_s and log (R_l) using the earthquakes with known magnitude and mapped fault rupture to calculate the rupture length of all historical events from the catalog (Fig 9e). We find

$$\log(R_l) = 2.29 * M_s - 12 \quad (3)$$

which is in good correspondence with literature values. This relation is used to infer the along-fault rupture length for the historical earthquakes without a mapped rupture (Table 5, column 4).

5. Results and discussion

5.1. Maximum observed magnitudes along different sections of the NAFZ

Fig. 10 shows the compiled historical earthquakes along the NAFZ for M > 6.6 plotted with longitude since the NAFZ generally strikes EW. Individual events are plotted together with the known or estimated rupture length (horizontal bars) and the respective magnitude uncertainty (vertical bars). The key information from the compiled historical

Table 4
Maximum segment length.

Lon (°)	Max. length (km)
26.3	31.6
26.4	47.4
27.15	39.5
27.5	23.7
27.8	31.6
28.075	51.35
28.525	43.45
29.1	47.4
29.4	55.3
29.9	63.2
30.1	31.6
30.475	43.45
31.175	27.65
31.75	47.4
32.325	43.45
32.65	7.9
32.925	35.55
33.525	19.75
33.79	25.28
34.15	31.6
34.695	68.73
35.56	77.42
36.26	45.82
36.6	31.6
36.95	23.7
37.55	86.9
38.475	90.85
39.38	50.56

Maximum coherent fault segment length per 0.6° longitude bins along the NAFZ from west to east. We considered individual fault segments as those with a minimum distance of 5 km to the adjacent fault segment. See text for details. Values are after Barka (1992). See also Fig. 8.

catalog is that there has not been a single M > 7.4 (or M > 7.6 assuming magnitude uncertainty) earthquake along the western part of the NAFZ during the entire examined 2300-year time period, expected to cover multiple earthquake cycles (Fig 10, Table 5). In contrast, magnitudes as large as M 7.8–8 are documented in the central and particularly in the eastern part of the fault zone. This observation is also supported by the various trenching studies at different segments and portions of the NAFZ, in that there is no indication at any of the western segments for a major earthquake not included in the 2300-year catalog. Although some early earthquakes from the catalog may be less well constrained, the three largest earthquakes that occurred within the instrumental period (i.e. 1939, 1943, 1999) agree with this tendency. The overall three largest earthquakes along the NAFZ that occurred during the 2300-year-long period considered here are the 1046, 1668, and 1939 events, the last one having a magnitude between M 7.8 (Grosser et al., 1998) and M 8.0 (Zabci et al., 2011; Ambraseys and Jackson, 1998).

Another feature in the results of Fig. 10 is that a much larger number of M < 7.5 earthquakes is observed in the western portion of the fault zone, while in the central part there is a substantial reduction of such events. This could reflect the inhomogeneous magnitude of completeness along the NAFZ which would be in accordance with settlement history, or alternatively could suggest a real decrease of M < 7.5 events resulting in larger recurrence periods and consequently larger events in the central part of the fault compared to the western part.

Plotting the maximum observed earthquake magnitudes within 0.4° longitude bins along the entire NAFZ from west to east for events with M > 6.8 covering the last 2300 years shows a systematic increase from west toward east (Fig. 11, Table 6). To test the stability of this observation, we account for variations of the seismogenic thickness along the fault from 14 km in the west to 16 km in the east (Grosser et al., 1998; Bulut et al., 2007; Yolsal-Çevikbilen et al., 2012, see Section 4) and the eastward increasing maximum segment length (Fig. 8). This is done by normalizing the maximum observed magnitudes along the fault for either parameter (Fig. 12). The normalized maximum magnitudes also show a clear trend being larger along the eastern NAFZ than along the western NAFZ. The fact that correcting for the rather strong variation in maximum segment length along the NAFZ from west to east has no substantial effect on the variation of maximum magnitudes indicates that the larger earthquakes along the eastern portion of the NAFZ reflect indeed multi-segment failure during the largest events (e.g. Mignan et al., 2015).

5.2. Relation between earthquake size and fault-zone parameters

To examine whether the observation of eastward increasing maximum earthquake magnitudes can be related to fault-zone parameters (age, cumulative offset, slip rate, and maximum segment length), we compare the observed magnitude distribution with the values for those parameters as summarized in Sections 3.1–3.4 (Figs. 5–8). The fault-zone age ranges from a maximum of 12–13 Ma at the easternmost part of the NAFZ to values probably as low as a few Ma around 30°E (Fig. 5, Table 1) (after Armijo et al., 1999; Hubert-Ferrari et al., 2002; Sengör et al., 2005; LePichon et al., 2015, and references therein). Between 40°E and 30°E and thus along ~800 km, the age shows a decrease from east to west in accordance with decreasing maximum magnitudes. West of 30°E, the maximum magnitudes are not further decreasing while the reported fault-zone age is 6–8 Ma (we note, however, that also much smaller values are reported, see Section 3.1). A more detailed differentiation of respective age variations between individual NAFZ fault strands is not reported and thus cannot be resolved here. In summary, the maximum observed magnitude scales with fault-zone age along most part of the NAFZ (30–40°E).

The correlation between maximum observed magnitudes and fault-zone age may reflect seismological evolution of the NAFZ with time. Extensive shear-box experiments were used (Tchalenko, 1970) to characterize the structural development of shear zones at the laboratory scale under three basic stages: (1) The peak stage where shear resistance is the highest and conjugate sets of Riedel shear zones start to form, (2) the post-peak stage where shear resistance decreases and "P" shears initiate symmetrically to the Riedel shears, (3) the residual stage where shear resistance becomes relatively stable along a single or several sub-parallel regions forming a shear deformation zone. Related observations associated with geometrical properties of natural fault zones are summarized in Ben-Zion and Sammis (2003), Papageorgiou (2003), and others. In addition, attempts were made to study repeated failure of individual patches and asperities during rock-deformation involving acoustic emission monitoring on the laboratory scale (Goebel et al., 2014). Based on our results of maximum observed earthquake magnitudes, the peak/post-peak stage may exist along the younger western (but east of the Marmara region) and central segments of the NAFZ, and the residual stage may characterize the older and well-developed eastern segments. This inference is consistent with rock fracturing experiments, where the ratio of smaller to larger laboratory earthquakes (the b-value of the frequency-magnitude statistics) decreases prior to the overall failure of the rock specimen, accompanying (micro-) structural changes during fault-zone propagation through previously intact material (Main et al., 1989; Lockner et al., 1991; Cowie and Scholz, 1992). The observation of an increasing maximum length of coherent fault segments from west to east fits well in this picture (Fig. 8).

The measurements of the cumulative offset across the NAFZ show large variations extending from a few tens to close to 90 km along most part of the fault zone (Armijo et al., 1999; Hubert-Ferrari et al., 2002; Sengör et al., 2005) (Fig. 6, Table 2). The only part with coherent values for the offset is the easternmost NAFZ (38–40°E) with offsets of 65–85 km. No systematic variation of cumulative fault-zone offset is observed along the NAFZ, but offsets <10 km are reported only for the western portion around 28°E (Fig. 6), although these might represent secondary fault strands and not the fault zone as a whole. We conclude

Table 5
Historical earthquake catalog.

Year	Lat [°N]	Lon [°E]	M_s	Rupture [km]	Reference
2014	40.3	25.4	6.8	(27)	Bulut (2015)
2003	39	40.5	6.4	(11)	Kalafat et al. (2009)
2003	39.5	39.8	6.2	(7)	Kalafat et al. (2009)
2000	40.7	33	6	(4)	Kalafat et al. (2009)
1999	40.7	30	7.3	(84)	Kalafat et al. (2009)
1999	40.8	31.2	7.0	50	Ambraseys (2002)
1999	40.7	30.0	7.3	98	Ambraseys and Jackson (1998), Ambraseys (2002)
1992	40.0	39.8	6.8	(27)	Grosser et al. (1998)
1992	39.7	39.6	6.2	(7)	Kalafat et al. (2009)
1983	40.3	27.8	6.1	(6)	Ambraseys (2002)
1975	40.5	26.1	6.5	(14)	Ambraseys (2002)
1971	39.0	40.7	6.8	38	Ambraseys and Jackson (1998)
1970	39.1	29.4	7.1	45	Ambraseys and Jackson (1998)
1969	39.1	28.4	6.1	(6)	Ambraseys and Finkel (1991)
1967	39.5	40.3	6.0	4	Ambraseys and Jackson (1998)
1967	40.7	30.7	7.2	71	Ambraseys (2002)
1966	39.3	41.2	6.2	7	Ambraseys and Jackson (1998)
1966	39.2	41.5	6.8	34	Ambraseys and Jackson (1998), Hartleb et al. (2003)
1965	40.4	26.1	5.9	(4)	Ambraseys and Finkel (1988)
1964	40.1	28.2	6.8	35	Ambraseys and Jackson (1998), Ambraseys (2002)
1963	40.7	29.0	6.4	5	Ambraseys and Jackson (1998)
1961	40.0	26.3	6.0	(4)	Kondorskaya and Ulomov (1999)
1960	40.1	39.5	5.9	(4)	Kondorskaya and Ulomov (1999)
1957	41.0	31.0	6.1	(6)	Ergin et al. (1967, 1971)
1957	40.7	31.0	7.1	66	Ambraseys and Jackson (1998), Ambraseys (2002)
1956	39.8	30.4	6.2	(7)	Ambraseys and Jackson (1998)
1954	41.1	36.3	6.2	(7)	Kondorskaya and Ulomov (1999)
1953	41.1	33.0	6.2	(7)	Kondorskaya and Ulomov (1999)
1953	40.1	27.4	7.1	55	Ambraseys and Jackson (1998)
1951	40.7	33.3	6.9	32	Ambraseys and Jackson (1998)
1951	40.9	32.9	6.5	(14)	Kalafat et al. (2009)
1949	39.4	40.8	6.9	(36)	Ambraseys and Jackson (1998)
1944	40.9	32.6	7.4	180	Ambraseys and Jackson (1998), Kondo et al. (2010)
1944	40.6	30.9	6.3	(9)	Ergin et al. (1967, 1971)
1944	39.0	29.4	6.0	(4)	Ambraseys and Finkel (1991)
1944	39.5	26.5	6.8	37	Ambraseys and Jackson (1998)
1943	41.0	35.5	7.7	280	Allen (1969),Stein et al. (1997), Ambraseys and Jackson (1998)
1943	40.7	30.5	6.4	(11)	Ambraseys (2002)
1942	40.9	36.5	6.0	(4)	Kalafat et al. (2009)
1942	40.8	35.1	5.9	(4)	Kondorskaya and Ulomov (1999)
1942	40.6	27.8	6.0	(5)	Kondorskaya and Ulomov (1999)
1942	40.7	36.3	7.1	47	Ambraseys and Jackson (1998)
1942	39.4	28.1	6.2	(7)	Ambraseys and Finkel (1991)
1941	40.8	27.8	6.1	(6)	Kondorskaya and Ulomov (1999)
1939	39.9	39.6	6.5	(14)	Kondorskaya and Ulomov (1999)
1939	39.0	26.9	6.5	(14)	Ambraseys and Finkel (1991)
1939	40.0	39.0	7.9	360	Ambraseys and Jackson (1998), Zabci et al. (2011)
1935	40.6	27.8	6.3	(9)	Ambraseys (2002)
1935	40.5	27.6	6.4	(11)	Ambraseys (2002)
1928	39.4	29.4	6.2	(7)	Ambraseys and Finkel (1988, 1991)
1924	39.1	30.1	6.0	(4)	Ambraseys and Finkel (1988, 1991)
1916	40.8	37.5	7.2	(67)	Ambraseys and Jackson (1998)
1919	41.2	33.2	6.0	(4)	Kondorskaya and Ulomov (1999)
1919	39.3	27.4	6.9	(34)	Ambraseys and Finkel (1991)
1912	40.7	27.0	7.3	54	Ambraseys and Finkel (1987), Ambraseys and Jackson (1998)
1912	40.8	27.5	6.2	(7)	Ambraseys and Jackson (1998)
1912	40.7	27.0	6.8	37	Ambraseys (2002)
1910	40.9	34.6	6.2	(7)	Kondorskaya and Ulomov (1999)
1909	40.2	37.8	6.4	15	Ambraseys and Jackson (1998)
1905	40.2	29.0	6.0	(4)	Kondorskaya and Ulomov (1999)
1905	40.6	28.3	5.9	(4)	Ambraseys and Finkel (1988), Ambraseys and Finkel (1991)
1903	40.6	29.0	5.9	(4)	Ambraseys and Finkel (1988), Ambraseys and Finkel (1991)
1901	40.0	41.5	6.0	(5)	Ambraseys (1997)
1901	39.4	26.7	5.9	(4)	Ambraseys and Finkel (1988, 1991)
1894	40.7	29.6	7.3	70	Ambraseys and Jackson (2000), Ambraseys (2002)
1893	40.5	26.2	6.9	41	Ambraseys and Jackson (1998), Ambraseys (2002)
1890	40.0	39.0	7.3	(84)	Öcal (1968)
1881	40.6	33.6	6.5	(14)	Turkish GSHAP Catalogue (2000)
1878	41.0	29.0	6.7	37	Kárník (1971)
1875	38.3	29.9	6.5	(14)	Ambraseys and Jackson (1998)
1873	40.5	37.8	6.5	(14)	Turkish GSHAP Catalogue (2000)
1866	39.2	41.0	7.2	45	Ambraseys (1997)
1866	38.5	41.0	6.8	(27)	Kondorskaya and Ulomov (1999)
1865	40.2	26.2	6.2	(7)	Papazachos and Papazachou (1997)
1863	40.5	29.1	6.4	(11)	Papazachos and Papazachou (1997)
1860	40.2	29.1	6.2	(7)	Papazachos and Papazachou (1997)
1860	40.5	26.0	6.1	(6)	Ambraseys and Jackson (2000), Ambraseys (2002)
1859	40.3	26.1	6.8	34	Ambraseys and Jackson (2000), Ambraseys (2002)
1859	40.0	41.3	6.5	(14)	Kondorskaya and Ulomov (1999)
1855	40.2	28.9	6.3	(9)	Ambraseys and Jackson (2000), Ambraseys (2002)
1855	40.1	28.6	7.1	59	Ambraseys and Jackson (2000), Ambraseys (2002)
1852	39.9	41.3	6.0	(4)	Kondorskaya and Ulomov (1999)
1850	40.1	28.3	6.1	(6)	Ambraseys and Jackson (2000)
1844	41.0	35.0	6.1	(6)	Kondorskaya and Ulomov (1999)
1841	40.9	29.1	6.1	(6)	Ambraseys and Jackson (2000)
1826	40.7	36.6	6.5	(14)	Turkish GSHAP Catalogue (2000)
1826	39.8	26.4	6.2	(7)	Ambraseys and Jackson (2000)
1809	40.0	27.0	6.1	(6)	Ambraseys and Jackson (2000)
1789	39.0	40.0	7.0	(43)	Kondorskaya and Ulomov (1999)
1784	39.5	40.2	7.6	(164)	Ambraseys and Jackson (1998)
1784	40.0	41.0	7.1	50	Grosser et al. (1998)
1766	40.8	28.2	5.8	(3)	Kondorskaya and Ulomov (1999)
1766	40.0	41.7	6.5	(14)	Turkish GSHAP Catalogue (2000)
1766	40.6	27.0	7.4	90	Ambraseys and Jackson (1998), Ambraseys (2002)
1766	40.8	29.0	7.1	58	Ambraseys and Jackson (1998), Ambraseys (2002)
1756	40.5	26.4	6.7	(22)	Papazachos and Papazachou (1997)
1754	40.8	29.2	6.8	36	Ambraseys and Jackson (1998), Ambraseys (2002)
1752	41.5	26.7	6.8	(27)	Ambraseys (2002)
1737	41.0	29.0	5.8	(3)	Kondorskaya and Ulomov (1999)
1737	40.0	27.0	7.0	49	Ambraseys and Jackson (1998), Ambraseys (2002)
1730	40.4	26.1	6.5	(14)	Papazachos and Papazachou (1997)
1719	40.4	26.0	6.7	(22)	Papazachos and Papazachou (1997)
1719	40.7	29.8	7.4	102	Klinger et al. (2003)
1718	40.3	41.5	6.5	(14)	Godzikovskaya (2000)
1707	40.2	26.4	6.8	(27)	Papazachos and Papazachou (1997)
1705	38.7	41.7	6.7	(22)	Kondorskaya and Ulomov (1999)
1690	40.9	29.0	6.3	(9)	Papazachos and Papazachou (1997)
1688	40.3	41.5	6.5	(14)	Godzikovskaya (2000)
1688	40.0	27.8	6.6	(17)	Papazachos and Papazachou (1997)
1685	39.0	41.0	6.7	(22)	Kondorskaya and Ulomov (1999)
1672	41.0	30.0	6.1	(6)	Kondorskaya and Ulomov (1999)
1672	40.0	26.0	6.1	(6)	Kondorskaya and Ulomov (1999)
1672	39.5	26.0	7.0	(43)	Ambraseys (2002)
1668	40.5	36.0	7.9	400	Ambraseys and Finkel (1995), Ambraseys and Jackson (1998)
1666	40.0	39.5	7.5	(131)	Ambraseys and Finkel (1995)
1660	40.0	41.3	6.5	(14)	Kondorskaya and Ulomov (1999)
1660	40.0	41.2	6.5	(14)	Godzikovskaya (2000)
1659	40.5	26.4	7.2	(67)	Ambraseys (2002)
1625	40.3	26.0	7.1	(53)	Ambraseys (2002)
1598	40.6	35.4	6.7	(22)	Turkish GSHAP Catalogue (2000)
1584	40.0	39.0	6.6	(17)	Arinci (1945)
1582	38.7	41.5	6.5	(14)	Turkish GSHAP Catalogue (2000)
1578	39.7	39.5	6.5	(14)	Turkish GSHAP Catalogue (2000)
1556	40.3	27.8	7.2	66	Ambraseys and Jackson (1998), Ambraseys (2002)
1543	39.7	39.5	6.5	(14)	Turkish GSHAP Catalogue (2000)
1510	40.9	35.2	7.0	(43)	Turkish GSHAP Catalogue (2000)
1509	40.9	35.2	7.4	(105)	Kondorskaya and Ulomov (1999)
1509	40.9	28.7	7.2	74	Ambraseys and Jackson (1998), Ambraseys (2002)
1481	39.9	40.4	7.7	(205)	Kondorskaya and Ulomov (1999)
1481	41.0	29.0	6.5	(14)	Papazachos and Papazachou (1997)
1457	39.7	39.5	6.9	(34)	Guidoboni and Comastri (2005)
1437	40.2	28.2	6.8	(27)	Papazachos and Papazachou (1997)
1422	39.7	39.5	6.7	(22)	Turkish GSHAP Catalogue (2000)
1419	41.0	34.0	7.5	(131)	Kondorskaya and Ulomov (1999)
1419	40.9	28.9	6.6	(17)	Papazachos and Papazachou (1997)
1419	40.4	29.3	7.2	(67)	Ambraseys (2002)
1363	38.7	41.6	6.9	(34)	Shebalin and Tatevossian (1997)
1354	40.7	27.0	7.4	(105)	Ambraseys (2002)
1343	40.9	28.0	7.0	(43)	Ambraseys (2002)
1343	40.7	27.1	6.9	(34)	Ambraseys (2002)
1308	39.7	39.5	6.5	(14)	Turkish GSHAP Catalogue (2000)
1296	40.5	30.5	7.0	(43)	Ambraseys (2002)

Table 5 (*continued*)

Year	Lat [°N]	Lon [°E]	M_s	Rupture [km]	Reference
1268	39.8	40.4	7.4	(105)	Tan et al. (2008)
1265	40.7	27.4	6.6	(17)	Papazachos and Papazachou (1997)
1254	40.0	38.3	7.2	(67)	Shebalin and Tatevossian (1997)
1254	39.7	39.5	7.5	(131)	Guidoboni and Comastri (2005)
1236	39.7	39.5	6.2	(7)	Guidoboni and Comastri (2005)
1231	41.0	28.6	6.9	(34)	Papazachos and Papazachou (1997)
1170	39.7	39.5	6.7	(22)	Turkish GSHAP Catalogue (2000)
1168	39.7	39.5	6.7	(22)	Turkish GSHAP Catalogue (2000)
1165	39.7	39.5	6.4	(11)	Guidoboni and Comastri (2005)
1135	39.7	41.7	6.4	(11)	Guidoboni and Comastri (2005)
1187	41.0	28.8	6.7	(22)	Papazachos and Papazachou (1997)
1065	40.4	30.0	6.8	(27)	Ambraseys (2002)
1063	40.9	28.3	6.5	(14)	Kondorskaya and Ulomov (1999)
1063	40.8	27.4	7.4	(105)	Ambraseys (2002)
1050	41.0	33.5	7.6	(164)	Ambraseys and Jackson (1998), Kozaci et al. (2011)
1046	39.0	40.0	7.8	(257)	Kondorskaya and Ulomov (1999)
1038	41.0	28.7	6.7	(22)	Papazachos and Papazachou (1997)
1011	39.7	39.5	6.5	(14)	Shebalin and Tatevossian (1997)
1010	40.6	27.0	7.4	(105)	Papazachos and Papazachou (1997)
995	39.0	40.0	7.0	(43)	Shebalin and Tatevossian (1997)
989	40.8	30.0	6.2	(7)	Guidoboni (1994)
989	40.8	28.7	7.2	(67)	Ambraseys (2002)
967	40.7	31.5	7.2	(67)	Ambraseys (1970), Barka (1996), Ambraseys and Jackson (1998)
894	40.0	27.0	7.4	(105)	Kozaci et al. (2011)
869	40.8	29.0	7.0	(43)	Ambraseys (2002)
869	41.0	29.0	6.2	(7)	Guidoboni (1994)
867	40.8	29.3	6.1	(6)	Kondorskaya and Ulomov (1999)
862	41.0	29.0	6.2	(7)	Guidoboni (1994)
860	40.8	28.5	6.8	(27)	Ambraseys (2002)
824	41.0	27.5	6.4	(11)	Tan et al. (2008)
815	41.0	28.5	7.4	(164)	Kondorskaya and Ulomov (1999)
802	39.7	39.5	6.5	(14)	Shebalin and Tatevossian (1997)
~800	40.0	39.0	7.5	(131)	Kozaci et al. (2011) (exact year not reported)
740	40.7	28.7	7.1	(53)	Ambraseys (2002)
602	38.7	41.6	6.0	(4)	Shebalin and Tatevossian (1997)
557	40.9	28.8	6.1	(6)	Kondorskaya and Ulomov (1999)
557	40.9	28.3	6.9	(34)	Ambraseys (2002)
554	40.7	29.8	6.9	(34)	Ambraseys (2002)
550	40.9	28.5	7.2	(67)	Kondorskaya and Ulomov (1999)
546	41.0	29.0	6.2	(7)	Tan et al. (2008)
543	40.4	35.8	6.2	(7)	Guidoboni (1994)
529	40.7	27.9	6.8	(27)	Guidoboni (1994)
484	40.5	26.6	7.2	(67)	Ambraseys (2002)
478	40.9	28.8	7.0	(43)	Kondorskaya and Ulomov (1999)
478	40.7	29.8	7.3	(84)	Ambraseys (2002)
464	40.4	27.8	7.3	(84)	Kondorskaya and Ulomov (1999)
460	40.1	27.6	6.9	(34)	Ambraseys (2002)
447	40.7	30.3	7.2	(67)	Ambraseys (2002)
437	40.8	28.5	6.8	(27)	Ambraseys (2002)
407	40.9	28.7	6.8	(27)	Ambraseys (2002)
368	40.5	30.5	6.8	(27)	Ambraseys (2002)
368	40.1	27.8	6.8	(27)	Ambraseys (2002)
362	40.4	29.7	6.2	(7)	Guidoboni (1994)
362	40.7	30.2	6.8	(27)	Ambraseys (2002)
358	40.7	30.2	7.4	(105)	Ambraseys (2002)
358	40.8	29.9	5.8	(3)	Kondorskaya and Ulomov (1999)
343	40.6	36.9	6.9	(34)	Guidoboni (1994)
268	40.7	29.9	7.3	(84)	Ambraseys (2002)
180	40.6	30.6	7.3	(84)	Ambraseys (2002)
180	40.5	31.0	7.3	(84)	Ambraseys (2002)
170	40.3	28.7	6.7	(22)	Tan et al. (2008)
160	40.0	27.5	7.1	(53)	Ambraseys (2002)
123	40.3	27.7	7.0	(43)	Ambraseys (2002)
121	40.5	30.1	7.4	(105)	Ambraseys (2002)
117	40.4	28.0	6.1	(6)	Kondorskaya and Ulomov (1999)
92	40.5	26.6	6.5	(14)	Kondorskaya and Ulomov (1999)
75	38.8	41.3	6.5	(14)	Shebalin and Tatevossian (1997)
69	40.6	29.9	6.1	(6)	Tan et al. (2008)
68	40.7	30.0	7.2	(67)	Ambraseys (2002)
32	40.5	30.5	7.0	(43)	Ambraseys (2002)
30	40.5	29.5	6.5	(14)	Kondorskaya and Ulomov (1999)
29	40.4	29.7	6.9	(34)	Tan et al. (2008)
-282	40.6	26.6	6.1	(6)	Kondorskaya and Ulomov (1999)
-287	40.6	26.9	6.8	(27)	Guidoboni (1994)
-342	40.4	26.6	6.1	(6)	Kondorskaya and Ulomov (1999)

Historical seismicity catalog for the NAFZ covering 2300 years compiled from various literature sources. Columns are year, latitude, longitude, magnitude (M_s), surface rupture length (in brackets those values calculated following the scaling derived from Fig. 2b), and reference for particular events, respectively.

that maximum observed magnitudes occur (in the eastern part of the NAFZ) where uniform large cumulative offsets are reported. However, no general relation between maximum observed earthquake magnitude and cumulative fault offset can be deduced for most of the NAFZ, partially due to the lack of consensus from the existing data. Still, since the western section of the fault displays significant branching, the cumulative offset may be distributed among them with individual values smaller than ~85 km.

Current slip rates at the NAFZ deduced from GPS measurements and thus covering the last few decades show an increase in the horizontal surface deformation from 20 mm/yr in the east to 25 mm/yr in the west (McClusky et al., 2000; Reilinger et al., 2006). The accelerated values toward the west are well-explained to result from the southwest-directed slab pull of the Hellenic subduction zone (e.g., Flerit et al., 2004) while the comparatively lower values in the east were explained to result from a reduced push of the northward moving Arabian Plate (e.g., Bulut et al., 2012). Reconstructing long-term slip rates and especially lateral variations along the NAFZ as a potential explanation for the non-uniformity of fault-zone age and offset variations is difficult and relies on few data points only (Fig. 7). Long-term slip rates are substantially smaller in the east (6.5 mm/yr over 13 Ma, Hubert-Ferrari et al., 2002) than in the west (14–17 mm/yr over 5 Ma, Armijo et al., 1999). Interestingly, this would result in a very good correlation between measured fault-zone offset and the cumulative offset calculated from the given slip rate of 6.5 mm/yr for the last 13 Ma (calculated offset: ~85 km, measured offset: 65–85 km) in the east, and as well for the western NAFZ assuming 17 mm/yr for the last 5 Ma (calculated offset: 85 km, measured offset: up to 75 km). Unfortunately, no long-term slip rates are reported for the longitude range 30–32°E where offsets are large and fault-zone age is probably youngest.

The obtained findings for the NAFZ indicate a relation between maximum observed earthquake magnitudes, fault-zone age, and maximum coherent segment length. No direct relation is found comparing

Table 6
Maximum earthquake magnitudes.

Ø Lon (°)	Min Lon (°)	Max Lon (°)	Ø Mag (Ms)	Min Mag (Ms)	Max Mag (Ms)
26	25.5	26.2	7.2	6.8	7.4
26.5	26	27.5	7.2	7	7.4
27	26.5	27.5	7.4	6.8	7.6
27.5	27.5	28	7.4	6.9	7.6
28	27.5	28.2	6.9	6.8	7.2
28.5	28	30	7.2	6.8	7.3
29	28.5	30	7.2	6.8	7.3
29.5	28.5	30	7.3	7.1	7.5
30	29.5	31	7.4	7.1	7.6
30.5	30	31	7.3	7.1	7.5
31	30	31.5	7.3	6.9	7.5
31.5	31	32	7.2	7	7.5
32.5	32	33.5	7.4	7.2	7.6
33	32.7	33.5	7.6	7.4	7.7
34	33.5	36	7.5	7.3	7.7
35	34	36.5	7.7	7.6	7.8
36	34	38	7.9	7.8	8
38.5	36.5	42	7.9	7.8	8

Maximum observed earthquake magnitude per 0.5° longitude bin along the NAFZ from west to east selected from the historical earthquake catalog shown in Table 5.

Table 7
Summary of observations on maximum observed earthquake magnitudes and fault-zone parameters along the NAFZ separated into the western, central and eastern portion.

NAFZ subregion	Max. magnitude	Fault-zone age	Cumulative offset	Current slip rate	Geological slip rate	Maximum segment length
Western (25–32°E)	M 7.4	0.2–8 Ma	Up to 85 km	25 mm/yr	17 mm/yr (5 Ma)	60 km
Central (32–36.5°E)	M 7.7	6–8.5 Ma	Up to 80 km	20–25 mm/yr	No data	80 km
Eastern (36.5–40°E)	M 8.0	up to 13 Ma	65–85 km	20 mm/yr	6.5 mm/yr (13 Ma)	90 km

Summary of observations on maximum observed earthquake magnitude and fault-zone parameters along the NAFZ separated into the western, central and eastern portion.

magnitudes with cumulative fault-zone offset and current or geological slip rates. Our results indicate that the entire 1200-km-long NAFZ can be subdivided into at least three main portions, each with different structural features which may affect the earthquake size (Table 7). The western NAFZ has a maximum observed earthquake magnitude of M 7.4 in combination with an age of up to 8 Ma, great diversity in cumulative offset measurements reaching 85 km, and a maximum segment length of 60 km. Slip rates in this region are 25 mm/yr (current) and 17 mm/yr (average for last 5 Ma).

All individual branches of the fault have coherent length segments typically not exceeding 20–40 km (e.g., Bohnhoff et al., 2013). The maximum observed earthquake magnitudes for this part of the NAFZ are limited to M 7.4. This suggests that further structural development may be needed before this portion of the NAFZ produces significantly larger earthquakes, as observed in the older eastern section (magnitudes up to ~8). However, if the cumulative offset is indeed as large as ~80 km in a single fault segment, earthquakes as large as 7.8 could be expected (Martínez-Garzón et al., 2015).

Along the central NAFZ earthquake magnitudes reach M 7.7 while the fault is up to 8.5 Ma old and the cumulative offset is reported to be up to 80 km. Unfortunately, no information on long-term slip rates are available for this part of the NAFZ (longest record covers 1–12 ky and reports 18 mm/yr, Hubert-Ferrari et al., 2002). The central portion of the NAFZ shows a partly well-developed fault zone whose fault segments started to merge toward longer coherent fault segments. This allows for advanced multi-segment failure due to smoothed stepovers, leading to earthquakes with magnitudes of up to M 7.6–7.8.

The eastern portion of the NAFZ represents a 12–13 Ma old mature fault zone. This is manifested also by the overall largest earthquake magnitudes along the NAFZ (up to M 7.8–7.9), the overall largest cumulative offset (up to 85 km), and individual coherent segments of the principal slip zone of up to 90 km length (Table 7).

In summary, our results indicate a correlation between the maximum earthquake size along the NAFZ and some fault-zone structural parameters (Table 7). A potential relation between these parameters was proposed and discussed for decades from generalized perspectives (e.g., Ben-Zion and Sammis, 2003, and references therein) for both laboratory (e.g. Tchalenko, 1970) and field scales (e.g. Wesnousky, 1988; Sengör et al., 2005; Wechsler et al., 2010). However, given the difficulty of obtaining reliable records of large earthquakes for time periods extending 100 years, there has been insufficient validation of these ideas with empirical field data. Applying these results to seismic hazard and risk of very densely populated areas such as the Istanbul metropolitan area suggest that this region is probably not expected to have a M ~ 8 type event in the next few millennia. However, the occurrence of the low-probability M > 9 Tohoku-Oki earthquake in 2011 indicates that such conclusions should be taken with care.

The newly compiled historical earthquake catalog for the NAFZ covering the last 2300 years with multiple earthquake cycles indicates an increasing maximum earthquake magnitude along the fault from east to west. This is not caused by variations in seismogenic thickness being slightly larger in the east (Fig. 12a). While the observation is based on few large earthquakes in the east, those M > 7.7 events, in particular the 1668 and 1939 events, are well-documented in historical records (e.g. the 1668 earthquake) or even instrumentally recorded (e.g. the 1939 Erzincan earthquake). For the western part of the fault with its long settlement history such large events can be ruled out to have occurred within the past 2300 years considered here.

5.3. Comparison to other transform faults

The correlation between the maximum observed earthquake magnitude and some structural parameters along different portions of the NAFZ (Figs 3-5) may apply to other strike-slip faults, taking into account the age of the fault (or the age of the independent segments), the length of the fault segments, and in some cases, the cumulative offset. To assess the potential generality of this correlation, we discuss the applicability

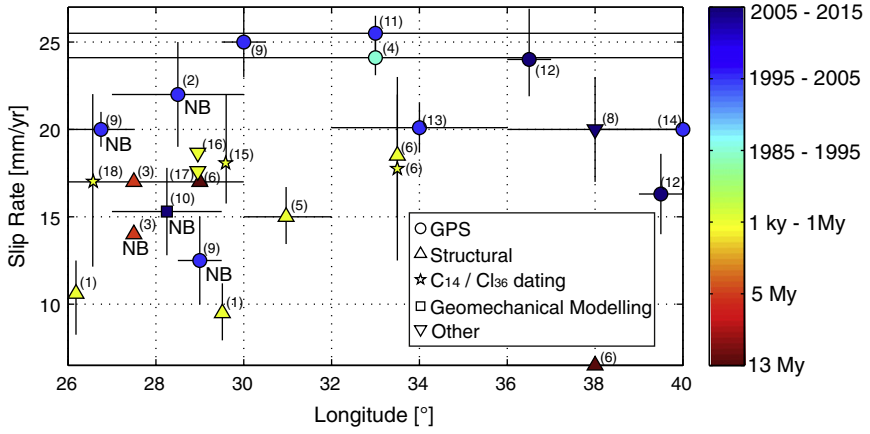

Fig. 7. Slip rates along the NAFZ. Slip rates along the NAFZ from west to east covering different along-fault portions and highly varying time periods extending from decades (GPS) to million years (structural data, InSAR). Superscripts represent the reference for the corresponding slip rate estimation: (1) Gasperini et al. (2011), (2) Straub et al. (1997), (3) Armijo et al. (1999), (4) McClusky et al. (2000), (5) Pucci et al. (2008), (6) Hubert-Ferrari et al. (2002), (7) Kozaci et al. (2007), (8) Walters et al. (2014), (9) Ergintav et al. (2014), (10) Hergert and Heidbach (2010), (11) Reilinger et al. (2006), (12) Tatar et al. (2012), (13) Yavaşoğlu et al. (2011), (14) Özener et al. (2010), (15) Kozacı et al. (2009), (16) Kurt et al. (2013), (17) Grall et al. (2013), (18) Meghraoui et al. (2012). Details and references are provided in Table 3. Values are generally in the range 15–25 mm/yr along the entire fault zone. The largest reported slip rates reflect the current GPS-derived deformation field and are observed for the central and western (as low as 30° longitude) sections of the fault. West of 30° toward the extensional Aegean domain the branching results in individual lower slip rates for the major NAFZ branches. NB refers to the northern NAFZ branch.

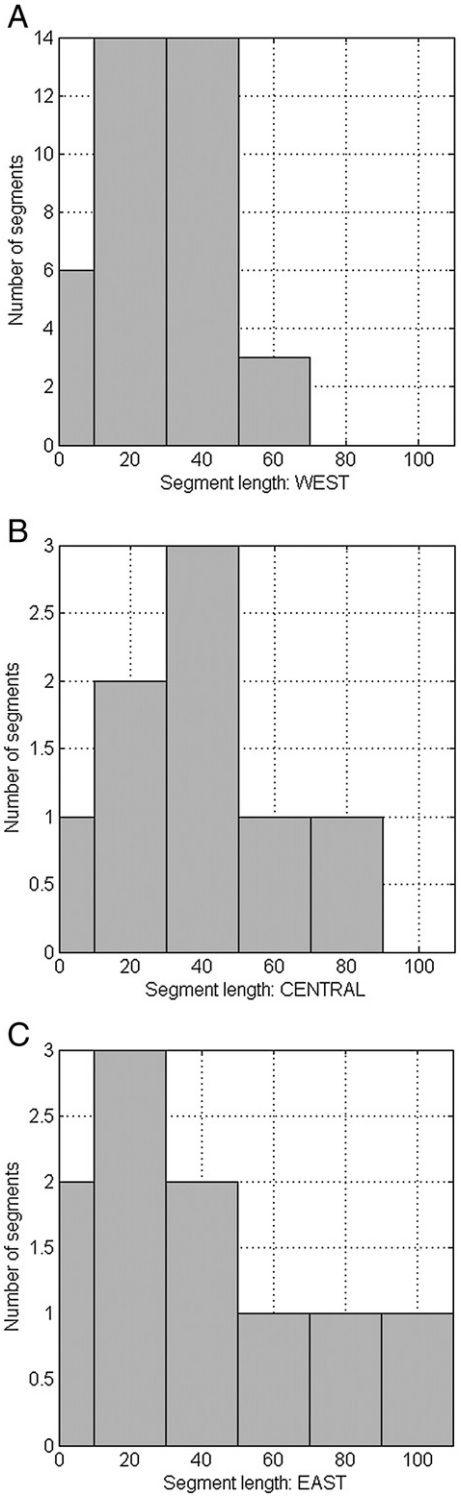

Fig. 8. Maximum segment length. Segment length for the western (A), central (B), and eastern (C) parts of the NAFZ after Barka (1992). The distribution shows that while segments lengths of up to ~40 km are observed along the entire fault, the maximum length increases from ~60 km in the west and ~80 km in the central part to close to 100 km in the east (for exact values see Table 4).

of our results to two other major continental transform fault zones: the San Andreas Fault (SAF) and the Dead Sea Transform (DST).

The SAF is probably the best-studied transform fault with regard to earthquakes occurring in the instrumental time period (the last ~100 years), imaged fault-zone structure and seismotectonic setting along most of its length. However, only comparatively limited information on historical earthquakes exists due to the written record dating back no longer than a few centuries. The SAF system represents a ~1300-km-long right-lateral strike-slip plate boundary between Pacific plate in the west and North American plate in the east. The relative plate motion is currently about 35 mm/yr based on GPS measurements (Thatcher, 1990). The SAF is not younger than 30 Ma in the north near Cape Mendocino and not younger than 20 Ma in the south near the Salton Sea (Atwater, 1970). However, the right-lateral motion is believed to have started about 12 Ma ago. Accordingly, the cumulative displacement along the SAF varies between 240 and 540 km, much larger than that of the NAFZ (up to 90 km). The SAF system developed within a ~100 km wide band being considerably narrower in the central (creeping section and Carrizo plain) portion and wider toward the edges (~80 km in the north around the San Francisco Bay and up to 150 km in Southern California). The SAF is basically split into five principal segments: (1) A ~300-km-long northern segment extending from Shelter Cove in the north toward the southern San Francisco Bay. The entire segment failed during the 1906 San Francisco earthquake (M_w7.9) with a ~430-km-long surface rupture (e.g. Ellsworth, 1990). (2) A ~170-km-long creeping section between San Juan Bautista and Parkfield. This segment accommodates a steady-state movement with only a little strain accumulation across the fault zone. Therefore, this segment of the SAF does not generate major ($M > 7$) earthquakes. (3) The ~30-km-long Parkfield segment of the SAF that repetitively failed in M~6 earthquakes in 1857, 1881, 1901, 1922, 1934, 1966, and 2004 (Ben-Zion et al., 1993; Hickmann et al., 2004; Harris and Arrowsmith, 2006). (4) The ~350-km-long central segment extending from Cholame near Parkfield to Cajon Pass near San Bernardino. It failed almost completely during the 1857 M_w 7.9 Fort Tejon earthquake (Ellsworth, 1990). (5) The ~300 km southern segment extending from Cajon Pass towards its end in the Salton Sea. It did not fail since the late 17th century and therefore it is believed to be overdue for a ~M 8.0 earthquake. Therefore, the longest coherent segments along the SAF are ~300 km long and either they have produced M ~ 8 earthquakes (1857 and 1906) or a large earthquake is expected. In summary, ~M8 earthquakes along the SAF in the last few centuries occurred along fault portions older than 10 Ma.

In contrast to the SAF, knowledge on the DST includes a well-documented historical earthquake catalog, owing to the long and continuous settlement history comparable to the Asia Minor region in Anatolia. However, there is less information on both fault-zone structure and instrumental seismicity for most of the DST sections. The left-lateral DST is bounding the African and Arabian Plates representing a ~1000-km-long north–south striking transform fault extending between the Gulf of Aqaba/Red Sea region in the south and the Taurus–Zagros compressional front in the north. It has been active since at least 25 Ma ago (Quennell, 1983) and current slip rates along the DST are between 1 and 10 mm/yr based on geomorphological observations, geodetic measurements, and plate kinematic considerations (Garfunkel, 1981; Meghraoui et al., 2003; Klinger et al., 2000). Recent GPS-based studies report average slip rates of 4–4.9 mm/yr (Reilinger et al., 2006). The DST transform has a cumulative offset of about 105 km in the south (Quennell, 1958; Weber et al., 2009) and 80 km in the north (Garfunkel, 1981). Due to the relatively high slip rates of 20–30 mm/yr at the NAFZ, the cumulative offsets of the NAFZ and DST are comparable, being 90 km in the east of the NAFZ and ~100 km at the DST.

While the cumulative offset along the DST is well defined, the record on long-term deformation rates at the DST are not well constrained. However, paleoseismological and archeological studies (Meghraoui et al., 2003) found significant evidence for historical earthquakes in the northern sector of the DST and this region appears to be in a seismic quiescence period for the last 830 years.

Due to the long settling history in the area of the DST, earthquake activity has been well reported over the past four millennia (Ben-Menahem, 1991). Strong events with magnitudes exceeding 7.2 occurred

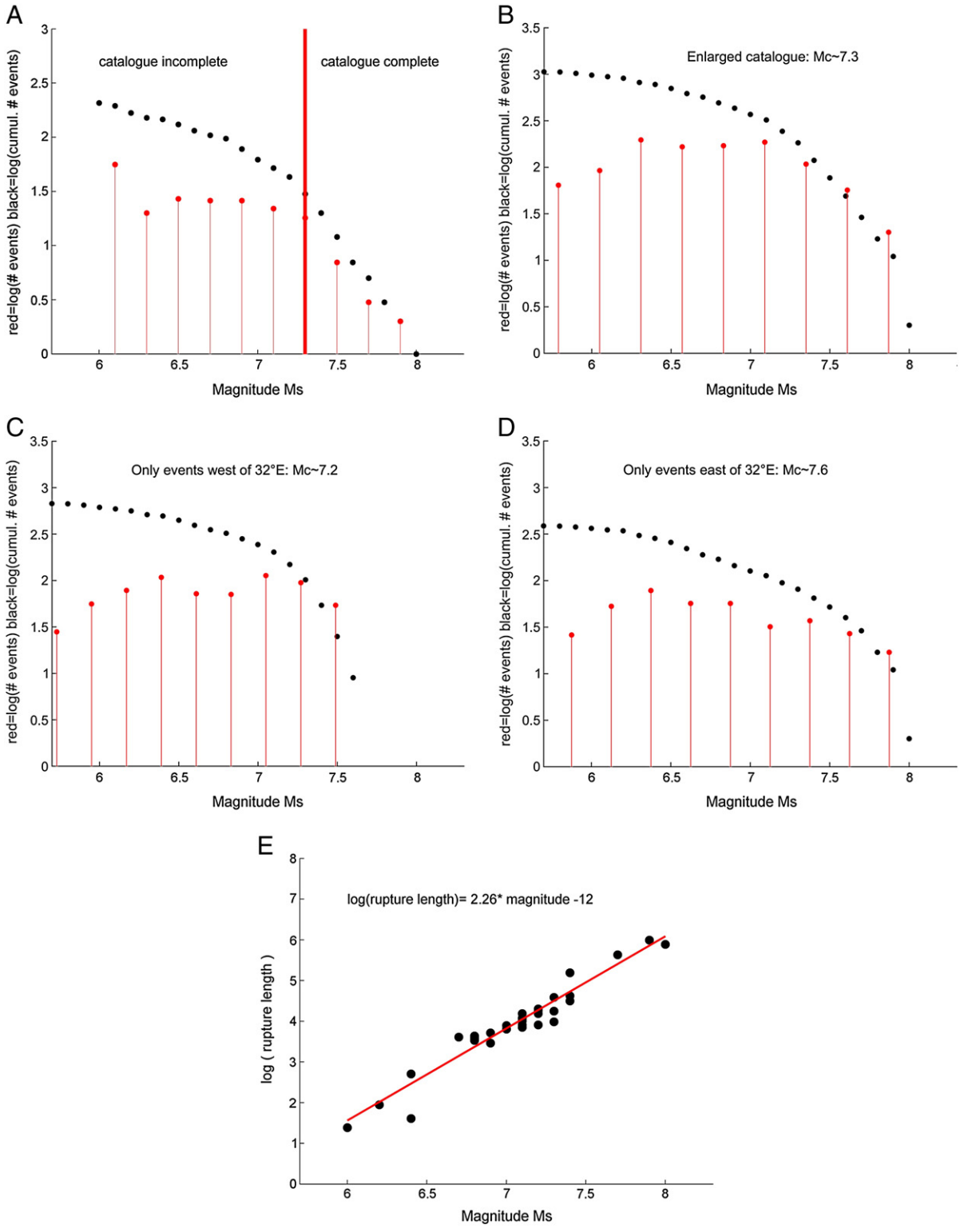

Fig. 9. Historical earthquake catalog. Magnitude-frequency distribution and rupture lengths for events from the historical earthquake catalog for the NAFZ presented in this study. A) Logarithmic number of events (red) and logarithmic cumulative magnitude frequency (black) for the entire historical earthquake catalog as provided in Table 4. The magnitude of completeness derived for the catalog is M_S 7.3 and is indicated by the red thick line. B) The same plot but for an artificially increased set of events incorporating standard deviations for magnitudes. This plot includes 1085 events and confirms Mc ~ 7.3. C) Magnitude-frequency distribution for events west of 32°E resulting in Mc ~ 7.2 for the western NAFZ including the Marmara region (690 events out of the 1085 events plotted in B). D) Magnitude-frequency distribution for events east of 32°E resulting in Mc ~ 7.6 for the central and eastern NAFZ (395 events out of the 1085 events plotted in B). E) Rupture length (R_l) plotted with magnitude for all events for which the along-strike rupture length is given in the literature (see Table 4). The regression line shows a reasonable good fit providing a base to calculate the rupture length for all other earthquakes of the catalog for which no measured rupture length is available.

along the northern section of the DST in the Bekaa valley close to the Yammouneh fault (Daeron et al., 2007) and toward the triple junction where the Arabian, African, and Anatolian Plates meet. The potentially strongest event reported for the DST is the Antiochia earthquake of 859 B.C., which occurred along the northern section (Ben-Menahem, 1991). However, its magnitude is heavily disputed in the literature with values

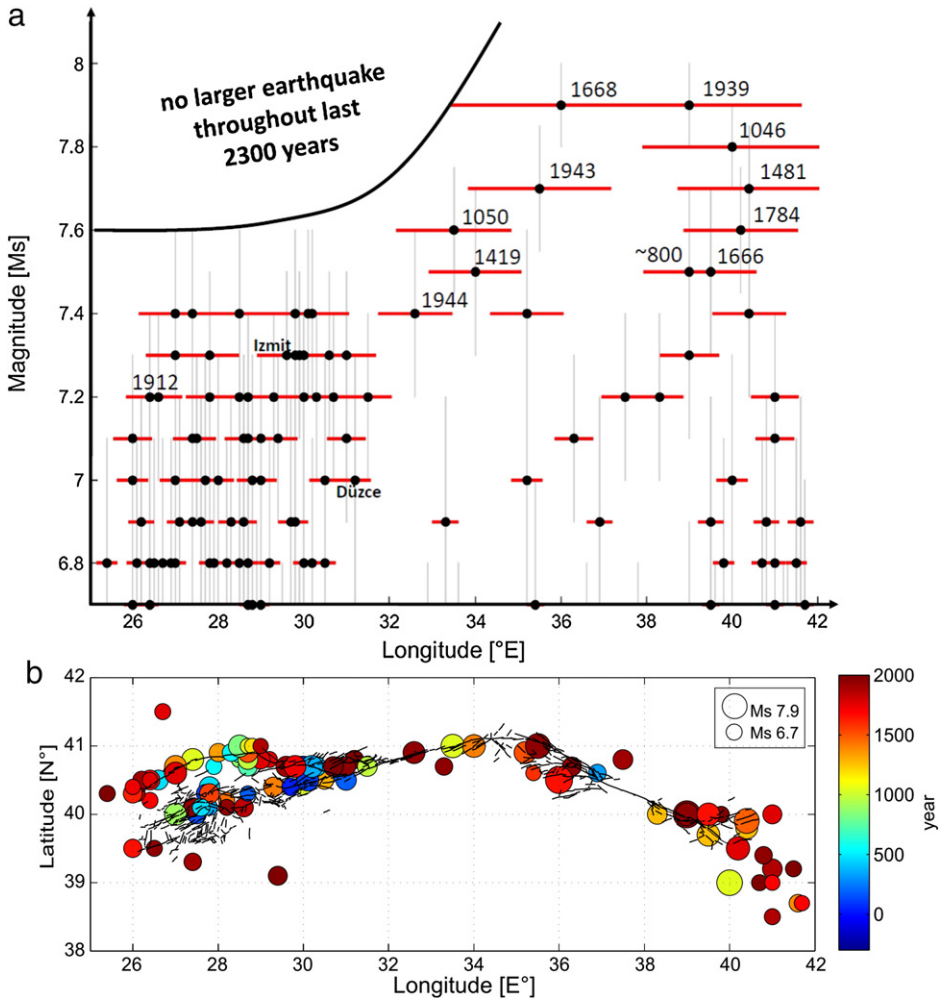

Fig. 10. Magnitude distribution along the NAFZ. a) Historical earthquakes with M > 6.6 along the NAFZ for the past 2300 years plotted with geographic longitude, i.e. along the east-west trending fault. The vertical gray lines represent the assumed magnitude errors as determined from the variety of given magnitudes for individual events of different size (±0.3, 0.2, 0.15, and 0.1 for magnitudes up to 7.0, 7.5, 7.7, and 8.0, respectively). The horizontal red lines represent the along-strike rupture length of the individual earthquakes calculated following the relation shown in Fig 2b. Numbers indicate the year of occurrence for the largest events and those during the 20th century. Izmit and Düzce refer to the two most recent M ≥ 7 earthquakes in northwestern Turkey in 1999. The entire historical earthquake catalog is listed in Table 4. b) Spatiotemporal distribution of the historical earthquake (M > 6.6) and mapped fault segments of the NAFZ with color indicating the year and circle size scaling with magnitude.

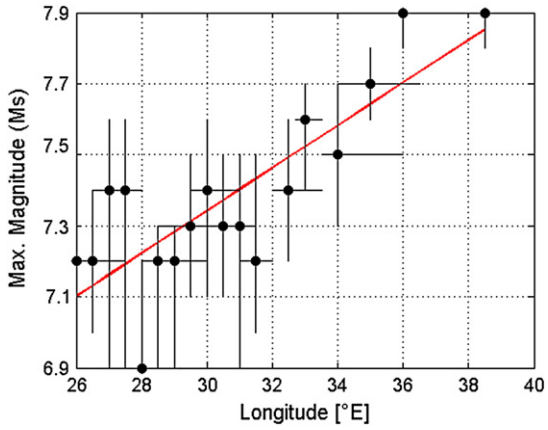

Fig. 11. Maximum observed magnitudes along the NAFZ. Maximum earthquake magnitudes (Ms) along the NAFZ from west to east. The red line is the linear regression curve showing a systematic increase from west to east. Maximum earthquake magnitude M was calculated per 0.4° longitude bins along the NAFZ. Values as in Table 5 and picked from the historical earthquake catalog shown in Table 4.

extending between M 7.0 and 8.0. Several studies report on a large number of earthquakes in the East during the years 859–860 B.C. (Ambraseys, 1971). These events were in part reported to be a single earthquake by many authors and often dated on the 8th of April 859 B.C., the beginning of the Mohammadan year 245 AH (Antonopoulos, 1980). Therefore, the grouping of several earthquakes as one single event may have resulted in an overestimation of the magnitude. We thus adopt the estimate of Meghraoui et al. (2003) giving to this event a magnitude range of 7.0–7.5. The largest event for which a consistent magnitude of 7.5 was reported occurred in 1759 in the Bekaa valley. In general, the historical earthquake catalog for the DST indicates several periods of pronounced and reduced seismic activity with a recurrence period for M7 events of 450–700 years (Khair et al., 2000).

In summary, taking into consideration that the magnitude of the 859 B.C. event is highly disputed, the maximum magnitude observed along the DST is approximately M 7.5 and, thus, smaller than the larger events along the NAFZ and SAF (up to M 8.0). In this sense, the DST seems to be not as developed as the NAFZ, and due to the tectonic complexity segments are not well defined. It is clear, however, that there has not been a single M > 7.5 earthquake along any section of the fault zone

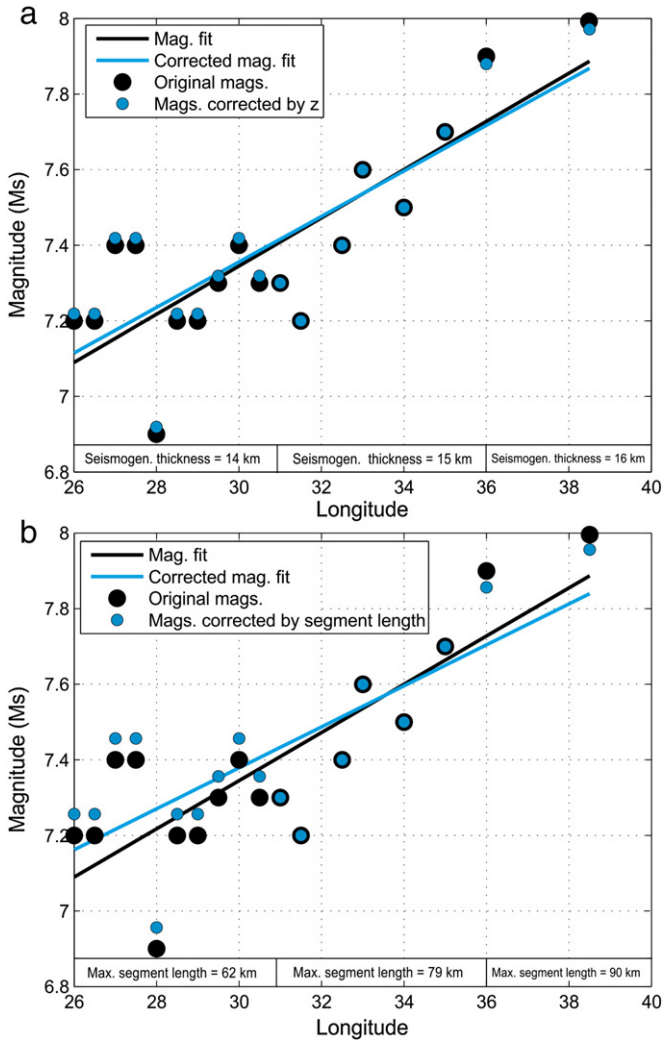

Fig. 12. Corrected maximum magnitudes. a) Maximum observed earthquakes magnitudes as in the historical earthquake catalog compiled in this study (black dots, as in Fig. 11 and magnitudes corrected for the variations in seismogenic thickness along the NAFZ (gray dots). Corrections were applied using three different values for the seismogenic thickness (western NAFZ: 14 km, central NAFZ: 15 km, eastern NAFZ: 16 km, see text for details) as follows: The maximum observed magnitudes (black dots) were converted as $M_s = M_w - 0.1$ (after Scordilis, 2006), then converted to moment magnitude using: $M_0 = 10.^(3.*(M_w + 6.03)./2)$ following Hanks and Kanamori (1979) and finally implementing the corresponding different seismogenic thickness in a normalized way with respect to the central part of the NAFZ (i.e. ±1 km relates to ±7%). Then, the process is repeated backwards to obtain the "corrected" magnitude (gray dots). b) Maximum observed magnitudes as in the here presented historical earthquake catalog (black dots, as in Fig. 4a) and magnitudes corrected for the variations in maximum coherent segment length as shown in Fig. 4d (gray dots). The corrected magnitudes accounting for the segment length in a normalized way were calculated as in a) by relative changes in fault segment length with respect to values at the central part of the NAFZ. In this case, the average maximum segment lengths are 62, 79, and 90 km for the western, central, and eastern NAFZ, respectively. For both corrections, the effect is minor compared to the actual variation in maximum observed magnitude along the fault.

with <5 Ma age reported for the last 2300 yrs. Although a catalog of historical and instrumental events for M > 7.3 is complete only for the NAFZ, the available records for both SAF and DST suggest that they could also follow the same relation between maximum earthquake size and fault age.

6. Conclusions

We compiled a catalog of historic seismicity for the entire North Anatolian Fault Zone covering a time period of 2300 years showing an increasing maximum earthquake magnitude along the fault from M ~ 7.4 in the west to M ~ 7.9 in the east. Comparing these results with fault zone parameters shows that the maximum earthquake magnitudes correlate with the duration of fault-zone activity along most of the fault, except for the greater Marmara region where the fault age may be up to 8 Ma and maximum magnitudes are stable at M ~ 7.4. The observed maximum magnitudes are also correlated with the length of maximum coherent fault segments. The results suggest that the larger Marmara–Istanbul region is not likely to have an M ~ 8 type event in the next few millennia, although this inference should be used with caution given the occasional occurrence of unexpectedly large events such as the M > 9 Tohoku-Oki earthquake in 2011.

No clear correlation between maximum earthquake magnitudes and the cumulative offset along the NAFZ was identified. Interestingly, the approximate constant measured upper limit offsets at the eastern and western NAFZ parts can be explained by the higher slip rates in combination with a younger fault age in the west and a smaller slip rate in combination with an older fault age in the east.

The observed results for maximum expected earthquake magnitudes in relation to fault-zone parameters along the NAFZ are consistent with available data for the San Andreas Fault and the Dead Sea Transform. The San Andreas Fault represents a well-developed structure capable of rupturing in up to M_s7.9 earthquakes, while the Dead Sea Transform is less structurally developed and does not have evidence for M ~ 8.0 events throughout the last 2300 years. The obtained results of maximum event size in relation to age of the fault and maximum length of coherent seismogenic segments could have important implications for earthquake hazard in different segments of strike-slip faults in close proximity to densely populated regions.

Acknowledgments

The study was funded by the Helmholtz Association in the frame of the "Young Investigators Group" ('From microseismicity to large earthquakes') (MB) and the Helmholtz Postdoc Programme (PMG). We thank Georg Dresen for comments on the manuscript, Maik Billing for editing the historical earthquake catalog, and Stefan Bentz for contributing to the design of Figs. 2–4. These figures were created with ArcGis and Esri GIS products. The manuscript benefitted from comments by Amir Sagy, an anonymous reviewer and editor Jean-Phillipe Avouac.

References

Akbayram, K., Sorlien, C.C., Okay, A.I., 2016. Evidence for a minimum 52 ± 1 km of total offset along the northern branch of the North Anatolian Fault in northwest Turkey. Tectonophysics http://dx.doi.org/10.1016/j.tecto.2015.11.026 ([online] Available from: http://www.sciencedirect.com/science/article/pii/S0040195115006563 (Accessed 4 January 2016, (n.d.))).

Aki, K., 1966. Generation and propagation of G waves from the Niigata earthquake of June 16, 1964, 2, Estimation of earthquake moment released, energy, and stress-strain drop from the G wave spectrum. Bull. Earthq. Res. Inst., Univ. Tokyo 44, 73–88.

Albini, P., Musson, R.M.W., Gomez Capera, A.A., Locati, M., Rovida, A., Stucchi, M., Viganò, D., 2013. Global historical earthquake archive and catalogue (1000—1903). GEM Technical Report. GEM Foundation, Pavia, Italy.

Allen, C.R., 1969. Active Faulting in Northern Turkey. Division Geol. Sci. Contr. no. 1577. Cal. Inst. Tech.

Altinok, Y., Alpar, B., Yaltirak, C., 2003. Sarköy-Mürefte 1912 earthquake's tsunami, extension of the associated faulting in the Marmara Sea. Turkey. J. Seismol. 7, 329–346.

Ambraseys, N.N., 1970. Some characteristic features of the Anatolian fault zone. Tectonophysics 9, 143–165.

Ambraseys, N.N., 1971. Some characteristic features of the Anatolian fault zone. Tectonophysics 9 (2), 143–165.

Ambraseys, N.N., 1997. The little-known earthquakes of 1866 and 1916 in Anatolia (Turkey). J. Seismol. 1 (3), 289–299.

Ambraseys, N.N., 2002. The seismic activity of the Marmara Sea region over the last 2000 years. Bull. Seismol. Soc. Am. 92, 1–18.

Ambraseys, N.N., Finkel, C.F., 1987. Seismicity of Turkey and Neighbouring Regions 1899–1915. Ann. Geophys. 5B, 701–726.

Ambraseys, N.N., Finkel, C.F., 1988. In: Lee, W.H.K., Meyers, H., Shimazaki, K. (Eds.), *Historical Seismograms and Earthquakes of the world*. Academic Press, San Diego, pp. 173–180.

Ambraseys, N.N., Finkel, C.F., 1991. Long-term seismicity of Istanbul and of the Marmara Sea region. Terra Nova 3, 527–539.

Ambraseys, N.N., Finkel, C.F., 1995. The Seismicity of Turkey and Adjacent Areas: A Historical Review, 1500–1800, Istanbul. 975-7622-38-9 (240p.).

Ambraseys, N.N., Jackson, J.A., 1998. Faulting associated with historical and recent earthquakes in the Eastern Mediterranean region. Geophys. J. Int. 133, 390–406.

Ambraseys, N.N., Jackson, J.A., 2000. Seismicity of the Sea of Marmara (Turkey) since 1500. Geophys. J. Int. 141, F1–F6.

Antonopoulos, J., 1980. Data from investigation on seismic sea-waves events in the Eastern Mediterranean from the birth of Christ to 500 AD. Ann. Geophys. 33 (1), 141–161.

Arinci, R., 1945. Arzda ve yurdumuzda zelzele bölgesi. Corumlu mecmuasi 4 (29), 897–903.

Armijo, R., Meyer, B., Hubert, A., Barka, A.A., 1999. Westward propagation of the North Anatolian fault into the northern Aegean: timing and Kinematics. Geology 27, 267–270.

Armijo, R., Meyer, B., Navarro, S., King, G., Barka, A.A., 2002. Asymmetric slip partitioning in the Sea of Marmara pull-apart:a clue to propagation processes of the North Anatolian Fault? Terra Nova 14, 80–86.

Armijo, R., et al., 2005. Submarine fault scarps in the Sea of Marmara pull-apart (North Anatolian Fault): implications for seismic hazard in Istanbul. G-cubed 6 (6), Q06009. http://dx.doi.org/10.1029/2004GC000896.

Atwater, T., 1970. Implications of plate tectonics for the Cenozoic tectonic evolution of western North America. Bull. Geol. Soc. Am. 81, 3513–3536.

Avouac, J.-P., 2015. From geodetic imaging of seismic and aseismic fault slip to dynamic modeling of the seismic cycle. Annu. Rev. Earth Planet. Sci. 2015 (43), 233–271.

Barka, A.A., 1992. The North Anatolian fault zone. Annales Tectonicae, Spec. Iss. VI, 164–195.

Barka, A.A., 1996. Slip distribution along the North Anatolian fault associated with the large earthquakes of the period 1939–1967. Bull. Seismol. Soc. Am. 86 (5), 1238–1254.

Barka, A., Akyüz, H.S., Cohen, H.A., Watchorn, F., 2000. Tectonic evolution of the Niksar and Tasova-Erbaa pull-apart basins, North Anatolian Fault Zone: their significance for the motion of the Anatolian Block. Tectonophysics 322, 243–264.

Barka, A.A., et al., 2002. The surface rupture and slip distribution of the 17 August 1999 Izmit Earthquake (M7.4), North Anatolian Fault. Bull. Seismol. Soc. Am. 92 (1), 43–60.

Ben-Menahem, A., 1991. Four thousand years of seismicity along the Dead Sea rift. J. Geophys. Res. 96 (B12), 20195–20216.

Ben-Zion, Y., 2008. Collective behavior of earthquakes and faults: continuum-discrete transitions, evolutionary changes and corresponding dynamic regimes, rev. Geophysics 46, RG4006. http://dx.doi.org/10.1029/2008RG000260.

Ben-Zion, Y., Lyakhovsky, V., 2006. Analysis of aftershocks in a lithospheric model with seismogenic zone governed by damage rheology. Geophys. J. Int. 165, 197–210. http://dx.doi.org/10.1111/j.1365-246X.2006.02878.x.

Ben-Zion, Y., Sammis, C.G., 2003. Characterization of Fault Zones. Pure Appl. Geophys. 160, 677–715.

Ben-Zion, Y., Rice, J.R., Dmowska, R., 1993. Interaction of the San Andreas fault creeping segment with adjacent great rupture zones and earthquake recurrence at Parkfield. J. Geophys. Res. 98, 2135–2144. http://dx.doi.org/10.1029/92JB02154.

Bohnhoff, M., Grosser, H., Dresen, G., 2006. Strain partitioning and stress rotation at the North Anatolian fault zone from aftershock focal mechanisms of the 1999 Izmit Mw=7.4 earthquake. Geophys. J. Int. 166, 373–385.

Bohnhoff, M., Harjes, H.-P., Meier, T., 2005. Deformation and stress regimes at the Hellenic subduction zone from Focal Mechanisms. J. Seismol. 9 (3), 341–366.

Bohnhoff, M., et al., 2013. An earthquake gap south of Istanbul. Nat. Commun. http://dx.doi.org/10.1038/ncomms2999.

Bulut, F., 2015. Different phases of the earthquake cycle captured by seismicity along the North Anatolian Fault. Geophys. Res. Lett. http://dx.doi.org/10.1002/2015GL063721.

Bulut, F., Bohnhoff, M., Aktar, M., Dresen, G., 2007. Characterization of aftershock-fault plane orientations of the 1999 Izmit (Turkey) earthquake using high-resolution aftershock locations. Geophys. Res. Lett. 34, L20306. http://dx.doi.org/10.1029/2007GL031154.

Bulut, F., Bohnhoff, M., Eken, T., Janssen, C., Kilic, T., Dresen, G., 2012. The East Anatolian Fault Zone: seismotectonic setting and spatiotemporal characteristics of seismicity based on precise earthquake locations. J. Geophys. Res. 117, B07304. http://dx.doi.org/10.1029/2011JB008966.

Cowie, P.A., Scholz, C.H., 1992. Physical explanation for the displacement-length relationship of faults using a post-yield fracture mechanics model. J. Struct. Geol. 14 (10), 1133–1148.

Daeron, M., Klinger, Y., Tapponnier, P., Elias, A., Jacques, E., Sursock, A., 2007. 12,000-year-long record of 10 to 13 paleoearthquakes on the Yammouneh fault, Levant fault system, Lebanon. Bull. Seismol. Soc. Am. 97 (3), 749–771.

Dewey, J.F., et al., 1989. Kinematics of the western Mediterranean. Geol. Soc. Lond. Spec. Publ. 45, 265–283.

Eberhart-Philips, D., et al., 2003. The 2002 Denali Fault earthquake, Alaska: a large magnitude, slip-partitioned event. Science 300, 1113–1118.

Ekström, G., Nettles, M., Dziewonski, A.M., 2012. The global CMT project 2004-2010: Centroid-moment tensors for 13,017 earthquakes. Phys. Earth Planet. Inter. 200, 1–9. http://dx.doi.org/10.1016/j.pepi.2012.04.002.

Ellsworth, W.L., 1990. In The San Andreas Fault System. In: Wallace, R.E. (Ed.), USGS, Washington, Professional Paper 1515, 6.

Ergin, K., Guclu, U., Aksay, G., 1971. A catalog of earthquakes for Turkey and surrounding area (1965-1970). Technical Univ. Istanbul, Inst.Phys. Earth, Publ,. 28 (91p.).

Ergin, K., Guclu, U., Uz, Z., 1967. A catalog of earthquakes for Turkey and surrounding area, 11 A.D. to 1964 A.D. Technical Univ. Istanbul, Inst. Phys. Earth, Publ. 24 (169p.).

Ergintav, S., Reilinger, R.E., Çakmak, R., Floyd, M., Çakır, Z., Doğan, U., King, R.W., McClusky, S., Özener, H., 2014. Istanbul's earthquake hot spots: geodetic constraints on strain accumulation along faults in the Marmara seismic gap. Geophys. Res. Lett. 41 (16), 5783–5788. http://dx.doi.org/10.1002/2014GL060985.

Field, E.H., et al., 2009. Uniform California earthquake rupture forecast, version 2 (UCERF 2). Bull. Seismol. Soc. Am. 99, 2053–2107.

Flerit, F., Armijo, R., King, G., Meyer, B., 2004. The mechanical interaction between the propagating North Anatolian Fault and the back-arc extension in the Aegean. Earth Planet. Sci. Lett. 224 (3(4)), 347–362. http://dx.doi.org/10.1016/j.epsl.2004.05.028.

Fraser, J., et al., 2009. A 3000-Year record of ground-rupturing earthquakes along the central North Anatolian Fault near Lake Ladik, Turkey. Bull. Seismol. Soc. Am. 99 (5), 2681–2703.

Garfunkel, Z., 1981. Internal structure of the Dead Sea leaky transform (rift) in relation to plate kinematics. Tectonophysics 80 (1), 81–108. http://dx.doi.org/10.1016/0040-1951(81)90143-8.

Gasperini, L., Polonia, A., Çağatay, M.N., Bortoluzzi, G., Ferrante, V., 2011. Geological slip rates along the North Anatolian Fault in the Marmara region. Tectonics 30 (6), TC6001. http://dx.doi.org/10.1029/2011TC002906.

Godzikovskaya, A.A., 2000. The catalogue of the Caucasus Earthquakes with M> 4.0 from ancient times to 2000. http://zeus.wdcb.ru/wdcb/sep/caucasus/welcomen.html.

Goebel, T.H.W., Candela, T., Sammis, C.G., Becker, T.W., Dresen, G., Schorlemmer, D., 2014. Seismic event distributions and off-fault damage during frictional sliding of saw-cut surfaces with pre-defined roughness. Geophys. J. Int. 196, 612–625. http://dx.doi.org/10.1093/gji/ggt401.

Grall, C., Henry, P., Thomas, Y., Westbrook, G.K., Çağatay, M.N., Marsset, B., Saritas, H., Çifçi, G., Géli, L., 2013. Slip rate estimation along the western segment of the main Marmara Fault over the last 405–490 ka by correlating mass transport deposits. Tectonics 32 (6), 2012TC003255. http://dx.doi.org/10.1002/2012TC003255.

Grosser, H., et al., 1998. The Erzincan (Turkey) earthquake (MS = 6.8) of March 13, 1992 and its aftershock sequence. Pure Appl. Geophys. 152, 465–505.

Grünthal, G., Wahlström, R., 2012. The European-Mediterranean Earthquake Catalogue (EMEC) for the last millennium. J. Seismol. 16, 535–570.

Guidoboni, E., 1994. Catalogue of ancient Earthquakes in the MEDITERRANEAN AREA up to the 10th Century. 1. INGV-SGA (504 pp.).

Guidoboni, E., Comastri, A., 2005. Catalogue of Earthquakes and Tsunamis in the Mediterranean Area from the 11th to the 15th Century. INGV-SGA, Bologna (1037 pp.).

Hanks, T., Kanamori, H., 1979. A Moment Magnitude Scale. J. Geophys. Res. 84 (B5), 2348–2350.

Harris, R.A., Arrowsmith, J.R., 2006. Introduction to the Special Issue on the 2004 Parkfield Earthquake and the Parkfield Earthquake Prediction Experiment. Bull. Seismol. Soc. Am. 96 (4B), S1–S10.

Harris, R.A., Dolan, J.F., Hartleb, R., Day, S.M., 2002. The 1999 Izmit, Turkey, Earthquake: A 3D Dynamic Stress Transfer Model of Intraearthquake Triggering. Bull. Seismol. Soc. Am. 92 (1), 245–255.

Hartleb, R.D., Dolan, F.F., Akyüz, H.S., Yerli, B., 2003. A 2000-year-long Paleoseismologic record of earthquakes along the Cantral North Anatolian Fault, from Trenches at Alayurt, Turkey. Bull. Seismol. Soc. Am. 93 (5), 1935–1954.

Herece, E., Akay, E., 2003. Atlas of North Anatolian Fault (NAF). General Directorate of Mineral Research and Exploration, Special Publication series-2, Ankara.

Hergert, T., Heidbach, O., 2010. Slip-rate variability and distributed deformation in the Marmara Sea fault system. Nat. Geosci. 3 (2), 132–135. http://dx.doi.org/10.1038/ngeo739.

Hickmann, S., Zoback, M.D., Ellsworth, W.L., 2004. Introduction to special section: preparing for the San Andreas Fault Observatory at Depth. Geophys. Res. Lett. 31, L12S01. http://dx.doi.org/10.1029/2004GL020688.

Hubert-Ferrari, A., et al., 2002. Morphology, displacement, and slip rates along the North Anatolian Fault, Turkey. J. Geophys. Res. 107 (B10), 2235.

Janssen, C., Bohnhoff, M., Vapnik, Y., Görgün, E., Bulut, F., Plessen, B., Pohl, D., Okay, A.I., Dresen, G., 2009. Tectonic evolution of the Ganos segment of the North Anatolian Fault (NW Turkey) deduced from multidisciplinary investigations. J. Struct. Geol. 31, 11–28.

Kalafat, D., Kekovalı, K., Güneş, Y., Yılmazer, M., Kara, M., Deniz, P., Berberoğlu, M., 2009. Türkiye ve Çevresi Faylanma-Kaynak Parametreleri (MT) Kataloğu (1938-2008): A Cataloque of Source Parameters of Moderate and Strong Earthquakes for Turkey and its Surrounding Area (1938-2008). Boğaziçi University Publication Bebek-İstanbul. (No=1026, 43p.).

Kárník, V., 1971. Seismicity of the European area. Springer Press.

Ketin, I., 1948. Über die tektonisch-mechanischen Folgerungen aus den großen anatolischen Erdbeben des letzten Dezenniums. Geol. Rundsch. 36, 77–83.

Khair, K., Karakaisis, G.F., Papadimitriou, E.E., 2000. Seismic zonation of the Dead Sea transform fault area. Ann. Geophys. 43 (1), 61–79.

Klinger, Y., et al., 2000. Slip rate on the Dead Sea transform fault in northern Araba valley (Jordan). Geophys. J. Int. 142 (3), 755–768.

Klinger, Y., et al., 2003. Paleoseismic evidence of characteristic slip on the western segment of the North Anatolian Fault. Turkey. Bull. Seismol. Soc. Am. 93 (6), 2317–2332.

Koçyiğit, A., 1988. Basic geological characteristics and total offset of the North Anatolian Fault Zone in Suşehri area, NE Turkey. METU Pure Appl. Sci. 22, 43–68.

Kondo, H., Özaksoy, V., Yildirim, C., 2010. Slip history of the 1944 Bolu–Gerede earthquake rupture along the North Anatolian fault system: implications for recurrence behavior of multisegment earthquakes. J. Geophys. Res. 115, B04316. http://dx.doi.org/10.1029/2009JB006413.

Kondorskaya, N.V., Ulomov, V.I., 1999. Special catalogue of earthquakes of the northern Eurasia. http://www.seismo.ethz.ch/static/gshap/neurasia/nordasiacat.txt.

Kozaci, Ö., Dolan, J., Finkel, R., Hartleb, R., 2007. Late Holocene slip rate for the North Anatolian fault, Turkey, from cosmogenic 36Cl geochronology: implications for the constancy of fault loading and strain release rates. Geology 35 (10), 867–870. http://dx.doi.org/10.1130/G23187A.1.

Kozacı, Ö., Dolan, J.F., Finkel, R.C., 2009. A late Holocene slip rate for the central North Anatolian fault, at Tahtaköprü, Turkey, from cosmogenic 10Be geochronology: Implications for fault loading and strain release rates. J. Geophys. Res. Solid Earth 114 (B1), B01405.

Kozaci, Ö., Dolan, J.F., Yönlü, Ö., Hartleb, R.D., 2011. Paleoseismic evidence for the relatively regular recurrence of infrequent, large-magnitude earthquakes on the eastern North Anatolian fault at Yaylabeli, Turkey. Lithosphere 3 (1), 37–54.
Kurt, H., et al., 2013. Steady late Quaternary slip rate on the Cinarcik section of the North Anatolian Fault near Istanbul, Turkey. Geophys. Res. Lett. 40.17, 4555–4559.
LePichon, X.L., Chamot-Rooke, N., Rangin, C., Sengör, A.M.C., 2003. The North Anatolian fault in the Sea of Marmara. J. Geophys. Res. 108. http://dx.doi.org/10.1029/2002JB001862.
LePichon, X.L., İmren, C., Rangin, C., Şengör, A.M.C., Siyako, M., 2014. The South Marmara Fault. Int. J. Earth Sci. 103 (1), 219–231. http://dx.doi.org/10.1007/s00531-013-0950-0.
LePichon, X.L., Sengör, A.M.C., Demirbag, E., Rangin, C., Imren, C., Armijo, R., Gorur, N., Cagatay, N., Mercier de Lepinay, B., Meyer, B., Saatcilar, R., Tok, B.X., 2001. The active main Marmara fault. Earth Planet. Sci. Lett. 192, 595–616.
LePichon, X.L., Şengör, A.M.C., Kende, J., İmren, C., Henry, P., Grall, C., Karabulut, H., 2015. Propagation of a strike slip plate boundary within an extensional environment: the westward propagation of the North Anatolian Fault. Can. J. Earth Sci. http://dx.doi.org/10.1139/cjes-2015-0129 ([online] Available from: http://www.nrcresearchpress.com/doi/abs/10.1139/cjes-2015-0129 (Accessed 4 January 2016)).
Lettis, W., Bachhuber, J., Witter, R., Brankman, C., Randolph, C.E., Barka, A.A., Page, W.D., Kaya, A., 2002. Influence of releasing step-overs on surface fault rupture and fault segmentation: examples from the 17 August 1999 I•zmit Earthquake on the North Anatolian Fault, Turkey. Bull. Seismol. Soc. Am. 92 (1), 19–42.
Lockner, D.A., et al., 1991. Quasi-static fault growth and shear fracture energy in granite. Nature 350, 39–42.
Main, I.G., Meredith, P.G., Jones, C., 1989. A reinterpretation of the precursory seismic b-value anomaly from fracture mechanics. Geophys. J. Int. 96, 131–138.
Martínez-Garzón, P., Bohnhoff, M., Ben-Zion, Y., Dresen, G., 2015. Scaling of maximum observed magnitudes with geometrical and stress properties of strike-slip faults. Geophys. Res. Lett., 2015GL066478. http://dx.doi.org/10.1002/2015GL066478.
McClusky, S., et al., 2000. Global positioning system constraints on plate kinematics and dynamics in the eastern Mediterranean and Caucasus. J. Geophys. Res. 105 (B3), 5695–5719. http://dx.doi.org/10.1029/1999JB900351.
Meghraoui, M., Aksoy, M.E., Akyüz, H.S., Ferry, M., Dikbaş, A., Altunel, E., 2012. Paleoseismology of the North Anatolian Fault at Güzelköy (Ganos segment, Turkey): size and recurrence time of earthquake ruptures west of the Sea of Marmara. Geochem. Geophys. Geosyst. 13 (4), Q04005. http://dx.doi.org/10.1029/2011GC003960.
Meghraoui, M., et al., 2003. Evidence for 830 years of seismic quiescence from palaeoseismology, archaeoseismology and historical seismicity along the Dead Sea fault in Syria. Earth Planet. Sci. Lett. 210 (1), 35–52.
Mignan, A., Danciu, L., Giardini, D., 2015. Reassessment of the maximum fault rupture length of strike-slip earthquakes and inference on Mmax in the Anatolian Peninsula, Turkey. Seismol. Res. Lett. 86 (3). http://dx.doi.org/10.1785/0220140252.
Öcal, N., 1968. Türkiyenin Sismisitesi ve Zelzele Coğrafyası , 1850-1960 Yılları İçin Zelzele Katoloğu. 8. Kandilli Rasathanesi Yayınları, İstanbul.
Okay, A., Tüysüz, O., Kaya, S., 2004. From transpression to transtension: changes in morphology and structure around a bend on the North Anatolian Fault in the Marmara region. Tectonophysics 391, 259–282.
Okay, A., et al., 1999. An active, deep marine strike-slip basin along the North Anatolian fault in Turkey. Tectonics 18 (1), 129–147.
Okumura, K., et al., 2004. Slip history of the 1944 segment of the North Anatolian Fault to quantify irregularity of the recurrence. Paper presented at the Geol. Soc. Am. Ann. Meeting, Denver, Colorado, 7 November 2004.
Özener, H., Arpat, E., Ergintav, S., Dogru, A., Cakmak, R., Turgut, B., Dogan, U., 2010. Kinematics of the eastern part of the North Anatolian Fault Zone. J. Geodyn. 49 (3–4), 141–150. http://dx.doi.org/10.1016/j.jog.2010.01.003.
Papageorgiou, A.S., 2003. The Barrier model and strong ground motion. Pure Appl. Geophys. 160, 603–634.
Papazachos, B., Papazachou, C., 1997. The Earthquakes of Greece. Ziti Publ., Thessaloniki, 356 pp., 1997. http://www.seismo.ethz.ch/static/gshap/turkey/seisgshap.prn.
Parsons, T., 2004. Recalculated probability of M≥7 earthquakes beneath the Sea of Marmara. J. Geophys. Res. 109, B05304. http://dx.doi.org/10.1029/2003JB002667.
Parsons, T., et al., 2000. Heightened odds of large earthquakes near Istanbul: an interaction-based probability calculation. Science 288, 661–665.
Pucci, S., De Martini, P.M., Pantosti, D., 2008. Preliminary slip rate estimates for the Düzce segment of the North Anatolian Fault Zone from offset geomorphic markers. Geomorphology 97 (3–4), 538–554. http://dx.doi.org/10.1016/j.geomorph.2007.09.002.
Quennell, A.M., 1958. The structural and geomorphic evolution of the Dead Sea rift. Quart. J. Geol. Soc. 114 (1-4), 1–24.
Quennell, A.M., 1983. Evolution of the Dead Sea Rift-a review. In: Abed, A.M., Khaled, H.M. (Eds.), Geology of Jordan. Proc. Jordanian Geol Sot. Conf., 1st (Amman). Jordanian Geol. Sot., Amman, pp. 460–482.
Reilinger, R., Toksoz, N., McClusky, S., Barka, A.A., 2000. 1999 Izmit, Turkey, earthquake was no surprise. GSA Today 10 (1), 1.6.
Reilinger, R., et al., 2006. GPS constraints on continental deformation in the Africa–Arabia–Eurasia continental collision zone and implications for the dynamics of plate interactions. J. Geophys. Res. 111, B05411. http://dx.doi.org/10.1029/2005JB004051.
Rockwell, T., Ragona, D., Seitz, G., 2009. Paleoseismology of the North Anatolian Fault near the Marmara Sea: implications for fault segmentation and seismic hazard. Geol. Soc. Spec. Publ. 316, 31–54.
Rockwell, T., et al., 2004. Paleoseismology of the 1912, 1944 and 1999 ruptures on the North Anatolian Fault: implications for long-term patterns of strain release. Paper presented at the Geol. Soc. Am. Ann. Meeting, Denver, Colorado, 7 November 2004.
Ruff, L.J., 1996. In: Bebout, G.E., Scholl, D.W., Kirby, S.H., Platt, J.P. (Eds.), Large Earthquakes in Subduction Zones: Segment Interaction and Recurrence Times, in Subduction Top to Bottom. American Geophysical Union, pp. 91–104 ([online] Available from: http://onlinelibrary.wiley.com/doi/10.1029/GM096p0091/summary (Accessed 25 August 2014)).
Scordilis, E.M., 2006. Empirical global relations converting Ms and mb to moment magnitude. J. Seismol. 10, 225–236.
Sengör, A.M.C., Görür, N., Saroglu, F., 1985. Strike-slip Faulting and Related Basin Formation in Zones of Tectonic Escape: Turkey as a Case Study. In Strike-slip Deformation, Basin Formation, and Sedimentation, Soc. Econ. Paleontol. Miner. Spec. Publ. 37, KT Biddle, N Christie-Blick, (227–64, in honor of J.C. Crowell).
Sengör, A.M.C., et al., 2005. The North Anatolian Fault: a new look. Ann. Rev. Earth Panet. Sci. 33, 37–112.
Seymen, İ, 1975. Kelkit vadisi kesiminde Kuzey Anadolu Fay zonunun tektonik özelliği. Dissertation thesis, Istanbul Technical University İTÜ.
Shebalin, N.V., Tatevossian, R.E., 1997. Catalogue of Large Historical Earthquakes of the Caucasus.
Sieh, K., et al., 1993. Near-field investigations of the Landers Earthquake sequence, April to July 1992. Science 260, 171–176.
Stein, R.S., Barka, A.A., Dieterich, J.H., 1997. Progressive failure on the North Anatolian fault since 1939 by earthquake stress triggering. Geophys. J. Int. 128, 594–604.
Stirling, M.W., Wesnousky, S.G., Shimazaki, K., 1996. Fault trace complexity, cumulative slip, and the shape of the magnitude-frequency distribution for strike-slip faults: a global survey. Geophys. J. Int. 124 (3), 833–868. http://dx.doi.org/10.1111/j.1365-246X.1996.tb05641.x.
Straub, C., Kahle, H.-G., Schindler, C., 1997. GPS and geologic estimates of the tectonic activity in the Marmara Sea region, NW Anatolia. J. Geophys. Res. 102 (B12), 27587–27601. http://dx.doi.org/10.1029/97JB02563.
Tan, O., Tapirdamaz, M.C., Yörük, A., 2008. The earthquake catalogues for Turkey. Turk. J. Earth Sci. 17, 405–418.
Tatar, O., et al., 2012. Crustal deformation and kinematics of the Eastern Part of the North Anatolian Fault Zone (Turkey) from GPS measurements. Tectonophysics 518–521, 55–62. http://dx.doi.org/10.1016/j.tecto.2011.11.010.
Tchalenko, J.S., 1970. Similarities between shear zones of different magnitudes. Geol. Soc. Am. Bull. 81 (6), 1625–1640.
Thatcher, W., 1990. In The San Andreas Fault System. In: Wallace, R.E. (Ed.), USGS, Washington, Professional Paper 1515, 7.
Turkish GSHAP Catalogue 2000, 2000. http://www.seismo.ethz.ch/static/gshap/turkey/seisgshap.prn.
Walters, R.J., Parsons, B., Wright, T.J., 2014. Constraining crustal velocity fields with InSAR for Eastern Turkey: limits to the block-like behavior of Eastern Anatolia. J. Geophys. Res. 119 (6), 5215–5234. http://dx.doi.org/10.1002/2013JB010909.
Weber, M.H., et al., 2009. Anatomy of the Dead Sea Transform from lithospheric to microscopic scale. Rev. Geophys. 47 (2), 457–478.
Wechsler, N., Ben-Zion, Y., Christofferson, S., 2010. Evolving geometrical heterogeneities of fault trace data. Geophys. J. Int. 182, 551–567. http://dx.doi.org/10.1111/j.1365-246X.2010.04645.x.
Wesnousky, S.G., 1988. Seismological and structural evolution of strike-slip faults. Nature 335, 340–343.
Westaway, R., 1994. Present-day kinematics of the Middle East and eastern Mediterranean. J. Geophys. Res. 99 (B6), 12071–12090.
Yaltırak, C., 2002. Tectonic evolution of the Marmara Sea and its surroundings. Mar. Geol. 190 (1), 493–529.
Yavaşoğlu, H., Tarı, E., Tüysüz, O., Çakır, Z., Ergintav, S., 2011. Determining and modeling tectonic movements along the central part of the North Anatolian Fault (Turkey) using geodetic measurements. J. Geodyn. 51 (5), 339–343. http://dx.doi.org/10.1016/j.jog.2010.07.003.
Yolsal-Çevikbilen, S., Berk Biryol, C., Beck, S., Zandt, G., Taymaz, T., Adiyaman, H.E., Arda Özacar, A., 2012. 3-D crustal structure along the North Anatolian Fault Zone in north-central Anatolia revealed by local earthquake tomography. Geophys. J. Int. 188 (3), 819–849. http://dx.doi.org/10.1111/j.1365-246X.2011.05313.x.
Zabci, C., Akyuzi, H.S., Karabacak, V., Sancar, T., Altunel, E., Gürsoy, H., Tatar, O., 2011. Turkish Palaeoearthquakes on the Kelkit Valley Segment of the North Anatolian Fault, Turkey: implications for the Surface Rupture of the Historical 17 August 1668 Anatolian Earthquake. Turk. J. Earth Sci. 20, 411–427. http://dx.doi.org/10.3906/yer-0910-48.